Evidence-Based Complementary and Alternative Medicine

Herbal Medicines and Arrhythmology: Risks and Opportunities

Lead Guest Editor: Luigi Gori
Guest Editors: Nicoleta Anca Sutan, Francesca Menichetti, and Simone Vanni

Herbal Medicines and Arrhythmology: Risks and Opportunities

Evidence-Based Complementary and Alternative Medicine

Herbal Medicines and Arrhythmology: Risks and Opportunities

Lead Guest Editor: Luigi Gori
Guest Editors: Nicoleta Anca Sutan, Francesca Menichetti, and Simone Vanni

Contents

Hindawi
Evidence-Based Complementary and Alternative Medicine
Volume 2022, Article ID 2022970, 13 pages
https://doi.org/10.1155/2022/2022970

Research Article

Effect of WenXin KeLi on Improvement of Arrhythmia after Myocardial Infarction by Intervening PI3K-AKT-mTOR Autophagy Pathway

Meng Lv, Ding Yang, Xiaodi Ji, Lixia Lou, Bo Nie, Jiuli Zhao, Aiming Wu, and Mingjing Zhao

Dongzhimen Hospital Affiliated to Beijing University of Chinese Medicine,
Key Laboratory of Chinese Internal Medicine of Ministry of Education and Beijing, Beijing 100700, China

Correspondence should be addressed to Aiming Wu; wam688@163.com

Received 18 May 2022; Revised 12 August 2022; Accepted 10 September 2022; Published 29 September 2022

Academic Editor: Anca Nicoleta Sutan

Background. Myocardial infarction (MI) is an acute and serious cardiovascular disease. Arrhythmia after MI can lead to sudden cardiac death, which seriously affects the survival outcome of patients. WenXin KeLi is a Chinese patent medicine for the treatment of arrhythmia in a clinic, which can significantly improve symptoms of palpitation and play an important role in reducing the risk of arrhythmia after MI. In this study, we aimed to explore the pharmacological mechanism of WenXin KeLi in protecting the heart. *Methods*. The MI model was established by ligating the left coronary artery and the ventricular fibrillation threshold (VFT) was measured by electrical stimulation. The expression of connexin43 (CX43) and autophagy-related protein were measured by Western Blot, and correlation analysis was conducted to study the relationship between cardiac autophagy, CX43, and arrhythmia in rats after MI. The effects of WenXin KeLi on arrhythmia, cardiac structure, and function in MI rats were respectively observed by electrical stimulation, cardiac gross section, Masson staining, and cardiac ultrasound. The effects of WenXin KeLi on the expression of phosphoinositide 3 kinase-protein kinase B-mammalian targets of rapamycin (PI3K-AKT-mTOR) autophagy pathway and CX43 were observed by Western Blot. *Results*. After 4 weeks of MI, the VFT in the model group was significantly reduced, the expression levels of yeast ATG6 homolog (Beclin1), microtubule-associated protein 1A/1B-light chain 3 (LC3II/LC3I), and p-CX43 (S368) significantly increased, the expression of sequestosome-1(P62) and CX43 significantly decreased. LC3II/LC3I and Beclin1 expression were significantly negatively correlated with the VFT, and the expression of P62 and CX43 were significantly positively correlated with the VFT. LC3II/LC3I and Beclin1 expression were negatively correlated with CX43 expression, while P62 expression was positively correlated with CX43 expression. WenXin KeLi could significantly increase the VFT, reduce the deposition of collagen fibers, and increase the index levels of the left ventricular end-diastolic anterior wall (LVEDAW), interventricular septum end-diastolic (IVSED), left ventricular end-systolic anterior wall (LVESAW), interventricular septum end-systolic (IVSES), left ventricular end-diastolic posterior wall (LVEDPW), left ventricular end-systolic posterior wall (LVESPW), left ventricular ejection fraction (LVEF) and left ventricular fractional shortening (LVFS), and reduce the index levels of the left ventricular end-diastolic dimension (LVEDD), left ventricular end-systolic dimension (LVESD), left ventricular end-diastolic volume (LVEDV) and left ventricular end-systolic volume (LVESV). WenXin KeLi could increase the expression of CX43, P62, AKT, p-PI3K, p-AKT (308), p-AKT (473), and p-mTOR and decrease the expression of LC3II/LC3I and Beclin1. *Conclusion*. WenXin KeLi can activate the PI3K-AKT-mTOR signaling pathway, improve cardiac autophagy and Cx43 expression in rats after MI, reduce the risk of arrhythmia after MI, and play a cardioprotective role.

1. Introduction

Epidemiological reports show that the prevalence of cardiovascular diseases in China is on the rise, cardiovascular disease is the leading cause of death in urban and rural residents [1]. Myocardial infarction (MI) is a serious type of cardiovascular disease. Cardiac structure and function after MI pathological changes and secondary arrhythmia complications, can lead to sudden cardiac death, and influence the outcomes in patients with long-term indicators [2]. Therefore, the study of the internal mechanism of arrhythmia events after MI is the key to improve the prognosis of MI. In recent years, autophagy has attracted much attention in cardiovascular research. Cardiac autophagy can be used not only as a protective factor for myocardial survival but also as a risk factor for cardiomyocyte death [3, 4], affecting the occurrence and development of diseases. The changes in autophagy after MI and its potential influence on complicated arrhythmias are worth studying. Connexin43 (CX43) is the most basic structural protein that constitutes the gap junction in the heart. The decreased expression of CX43 will directly lead to the electrical conduction disorder between myocardial cells [5]. Autophagy is one of the main pathways of protein degradation, and excessive activation of autophagy will accelerate CX43 degradation and even lead to myocardial cell death [6]. Therefore, changes in autophagy level and CX43 expression may be associated with arrhythmia after MI, but it still a lack of experimental verification.

Many evidence-based clinical studies have shown that Traditional Chinese Medicine (TCM) plays a role in improving ischemic diseases. WenXin KeLi is a Chinese herbal compound and is mainly composed of *Codonopsis pilosula*, *Polygonatum kingianum*, *Panax notoginseng*, *Amber*, and *Nardostachy jatamansi* (the percentage is 15 : 20 : 3:2 : 10), which is the first antiarrhythmic Chinese medicine to be approved by the Chinese state. Results of systematic pharmacological studies on WenXin KeLi extract showed that it reduced malignant arrhythmias and shortened RR, PR, and QT intervals [7]. Systematic review and meta-analysis results have proved that WenXin KeLi can effectively reduce the occurrence of complications after MI, play a heart-protective role and prolong the survival period of patients [8, 9]. Whether its mechanism of protecting the heart and reducing the risk of arrhythmia after MI is related to the intervention of cardiac autophagy and improvement of gap junction protein expression is a scientific question worthy of further study. The PI3K-AKT-mTOR pathway is a widely studied autophagy pathway [10]. Our study intends to explore the changes in cardiac autophagy, myocardial CX43 expression levels, and their correlation with arrhythmia in MI rats. On this basis, the cardiac protection mechanism of WenXin KeLi improving CX43 expression and reducing the risk of arrhythmia after MI was further analyzed from the perspective of the PI3K-AKT-mTOR autophagy pathway, hoping to provide new experimental evidence for revealing the molecular mechanism of TCM in the prevention and treatment of arrhythmia after MI.

2. Materials and Methods

2.1. Animal Model. Male Sprague-Dawley rats (body mass 200g ± 20 g) were purchased from Beijing Weitong Lihua Laboratory Technology Co., Ltd. (license number SCXK2016-0006), and raised in the Environmental Animal Barrier Room of the Key Laboratory of the Ministry of Internal Medicine of Traditional Chinese Medicine. All animal experiments were approved by the Experimental Animal Ethics Committee of Dongzhimen Hospital. According to reference [11], the rat model of myocardial infarction was established by ligation of the anterior descending branch of the left coronary artery. Immediately after ligation, ischemia and whitening of the anterior wall of the left ventricle were observed, the ST segment was significantly elevated, and the pathological *Q* wave was observed 24 hours after the operation.

2.2. Group Administration. The pathological *Q* waves with postoperative 24 hours in the anterior wall V3–V6, lateral wall I, AVL lead, and the anteroseptal wall V1 or V2 were used as grouping criteria [12]. The animals were randomly divided into the model group, the metoprolol group, the low dose of WenXin KeLi (WXKL-LD) group, and the high dose of WenXin KeLi (WXKL-HD) group. The sham group was only threaded without ligation. Each group had 8 rats. The doses of WenXin KeLi and the metoprolol group were converted according to the equivalent dose conversion method of reference [13]. WenXin KeLi (5 g per capsule) was provided by Buchang Pharmaceutical Co., Ltd. (Shandong, China), and metoprolol Tartrate tablets (25 mg per tablet) were provided by AstraZeneca Pharmaceutical Co., Ltd. (Jiangsu, China). According to the group, all rats were treated via intragastric administration (1.35 g/Kg/d in the WXKL-LD group, 2.25×10^{-3} g/Kg/d in the Metoprolol group, 2.7 g/Kg/d in the WXKL-HD group). Intragastric administration was started 24 hours after the operation, once a day, for 4 weeks. The sham group and model group were given normal saline.

2.3. Cardiac ultrasound. Four weeks after the operation, the rats were anesthetized by intraperitoneal injection, and the skin was prepared in a large area of the chest and abdomen. The rat was fixed on the ultrasound test table, and the M-mode curve imaging was performed at the left ventricle beside the sternum guided by two-dimensional ultrasound (small animal ultrasound imaging system Vevo2100, Toronto, Canada). Left ventricular end-diastolic anterior wall (LVEDAW), interventricular septum end-diastolic (IVSED), left ventricular end-diastolic posterior wall (LVEDPW), left ventricular end-diastolic dimension (LVEDD), left ventricular end-diastolic volume (LVEDV), left ventricular end-systolic anterior wall (LVESAW), interventricular septum end-systolic (IVSES), left ventricular end-systolic posterior wall (LVESPW), left ventricular end-systolic dimension (LVESD), left ventricular end-systolic volume (LVESV), left ventricular ejection fraction (LVEF), and left ventricular fractional shortening (LVFS)

were measured. At least three consecutive cardiac cycles were selected for all the original measurements and the average values were taken.

2.4. Cardiac macroscopic. Four weeks after the operation, the rats were anesthetized. The chest cavity was opened, and the heart was taken out and placed into precooled 4°C normal saline to wash away the residual blood. The heart was placed on a low-temperature container, sterilized gauze was used to absorb the liquid, and a general picture of the heart was taken. The left atrial appendage, right atrium, and right ventricle were cut off by ophthalmic scissors, and the tissue blocks of 4 mm were cut at the largest cross-section of the heart and soaked in a 4% tissue fixative solution. After fixation for 24 hours, the tissue was treated with a fully automatic closed tissue dehydrator and then embedded in paraffin to make a paraffin section of 4 μm thickness.

2.5. Masson staining. Paraffin sections of rat myocardial tissue were put into xylene first, then put in the gradient alcohol. Masson staining was performed according to the instructions of the staining kit (D026-1, Nanjing, China). The sections were stained with nuclear dye solution for 60 seconds, rinsed with flushing solution, stained with pulp dye solution for 50 seconds, rinsed with flushing solution, separated with color separation solution for 8 minutes, and directly stained with a redyeing solution for 5 minutes, finally washed with anhydrous alcohol, dried in the ventilation place and sealed. The collagen volume fraction (CVF) was analyzed by Image J software. 8 sections were selected from each group, and 3 nonoverlapping visual fields were collected from each slice for statistical analysis.

2.6. The ventricular Fibrillation Threshold (VFT) Detecting. The rats were anesthetized by intraperitoneal injection. Endotracheal intubation was performed, the ventilator was connected to assist respiration, and the biological function system (BL-420S, Chengdu, China) was connected. Then start the system software, select the menu "Input signal/Channel 1/ECG," and the ECG waveform will appear. Open the rat chest with scissors along the fourth and fifth intercostal lines and expose the heart. The positive pole of the stimulation electrode was hooked at the apex of the heart, and the negative pole was hooked at a distance of 3 mm away from the positive pole near the bottom of the heart. The electrical stimulation conditions (crude voltage, string stimulation, string length of 10 stimulation waves, initial intensity 1V) were set. After the pattern was stabilized, electrical stimulation was started, the condition of ventricular fibrillation induced by electrical stimulation within 15V was recorded, and the voltage value of ventricular fibrillation induced for the first time was taken as the threshold value of ventricular fibrillation.

2.7. Immunofluorescence detecting. The paraffin sections were placed on a 60°C slide drier for 1 hour (HI1220, LEICA, Germany), then put into xylene I, xylene II, xylene III for 15 minutes each, anhydrous ethanol I, anhydrous ethanol II, 95% ethanol I, 95% ethanol II, 90% ethanol, 80% ethanol and 70% ethanol for 5 minutes each, and rinsed with PBS buffer 3 times for 5 minutes each. Put the sections into the incubator box containing sodium citrate antigen repair solution and 98°C heat preservation for 20 minutes. After natural cooling, sections were rinsed with PBS buffer 3 times for 5 minutes each, put into 0.3% PBST for 20 minutes, and rinsed with PBS buffer 3 times 5 minutes each. Then rat heart tissue on the section was added to 100 μL 8% donkey serum sealing solution and incubated at 37°C for 30 minutes. Without washing, the CX43 antibody (Abcam company, product number: ab11370) diluted by 5% donkey serum was added, overnight at 4°C. Avoid light operation, add fluorescent secondary antibody on the tissue, incubate at 37°C for 1 hour, wash with PBS buffer solution 3 times, each time for 5 minutes, and add DAPI sealing agent. Images were collected by fluorescence microscope to observe the expression changes of CX43 proteins in each group.

2.8. Western Blot Detecting. About 20 mg of tissue was removed from the marginal area of ventricular infarction of the rat, and adding 200 μL of RIPA lysate according to the proportion of 1 : 10 with fully ultrasonic homogenate. After standing for 20 minutes, the supernatant was removed by centrifugation at a low temperature. Protein concentration was determined using a BCA kit, adjusted to 4 μg/μL, and stored at −20°C. SDS-PAGE gel electrophoresis was performed with a sample loading volume of 10 μL per group and a constant flow of 200mAn. The proteins were transferred to the PVDF membrane and sealed at room temperature for 1 hour. After washing membranes with TBST, the diluted primary antibody was added and incubated at 4°C overnight. The dilution ratios of GAPDH, CX43, LC3, P62, and Beclin1 antibodies were 1 : 20000, 1 : 8000, 1 : 1500, 1 : 5000, and 1 : 5000, respectively. The secondary antibody was incubated at room temperature for 1 hour, and the protein band can be visualized by chemiluminescene. ImageJ was used to analyze the protein band and calculate the relative expression levels of each group of proteins.

2.9. Confocal detecting. The staining procedure of the paraffin section was the same as that of experiment 7. The mixture of LC3 antibody and CX43 antibody was dropped for each section, and the dilution ratio of LC3 and CX43 were 1 : 300 and 1 : 300 respectively. After staining, images were collected in a darkroom under a confocal laser scanning microscope (TSC SP8 X, LEICA, Germany). The average fluorescence intensity of each protein expression was analyzed by Image J.

2.10. Statistical Analysis. SPSS software was used for statistical analysis, and the measurement data were expressed by means ± standard deviation. First, a normality test was carried out. One-way ANOVA was used for normal variables. When the variables were normal and homogeneous, the LSD method was used for inter-group comparison;

Dunnett's T3 method was used when variance was uneven, and the nonparametric rank sum test was used when non-normal. Pearson correlation analysis was used for the correlation test. $P < 0.05$ was considered statistically significant.

3. Results

3.1. Study on the Correlation between Cardiac Autophagy and Arrhythmia in Rats with MI. Four weeks after the operation, the VFT in the model group was significantly lower than that in the sham group (Figure 1(a)). Western Blot results showed that the protein expression of Beclin1 and LC3II/LC3I significantly increased and the expression of P62 protein significantly decreased in the model group (Figure 1(b)). In the model group, the expression of CX43 protein decreased significantly, while the expression of p-CX43 (S368) protein increased significantly (Figure 1(c)). Correlation analysis showed that there was a significant positive correlation between CX43 protein expression and the VFT ($r = 0.92$). The correlation coefficients between the expression of autophagy-related proteins LC3 II/LC3 I, Beclin1, P62, and CX43 protein were −0.76, −0.81, and 0.75, respectively, indicating that there was a significant negative correlation between LC3 II/LC3 I, Beclin1 protein expression and CX43 protein expression, and a significant positive correlation between P62 protein expression and CX43 protein expression. The correlation coefficients between the expression of autophagy-related proteins LC3II/LC3 I, Beclin1, P62, and the VFT were −0.84, −0.82, and 0.86, respectively, indicating that there was a significant negative correlation between the expression of LC3II/LC3 I, Beclin1 protein and the VFT, and a significant positive correlation between P62 protein expression and the VFT (Figure 1(d)).

3.2. Effects of WenXin KeLi on Arrhythmia and Cardiac structure and Function in Rats with MI. Four weeks after the operation, the VFT induced by electrical stimulation in the WXKL-HD group and metoprolol group was significantly higher than that in the model group (Figure 2(a)). Compared with the sham group, the color of the infarcted area of the left ventricle became white, the ventricular wall became thinner and collapsed widely and the ventricular cavity enlarged in the model group. Compared with the model group, the white fibrotic area in the marginal zone of ventricular infarction decreased and the area of the ventricular cavity decreased in each drug group (Figure 2(b)). Masson staining showed that there was a small amount of collagen in the myocardial space of the sham group. Compared with the sham group, the model group had a large amount of collagen deposition in the myocardial space, myocardial fibrosis was obvious, and the myocardial CVF was significantly increased. Compared with the model group, the CVF in the WXKL-LD group, WXKL-HD group, and metoprolol group decreased significantly (Figure 2(c)). The results of ultrasound showed that compared with the model group, LVESAW and IVSED increased, and LVEDD and LVEDV decreased significantly in the WXKL-LD group. In the WXKL-HD group and metoprolol group, LVEDAW, LVESAW, IVSED, IVSES, LVEDPW, LVESPW, LVEF, and LVFS increased significantly, LVEDD, LVESD, LVEDV, and LVESV decreased significantly (Figure 2(d)).

3.3. Effect of WenXin KeLi on CX43 Protein Expression. Compared with the model group, after four weeks of treatment with WenXin KeLi, the expression of CX43 protein increased while there was no statistical difference in the expression of p-CX43(S368) (Figure 3(a)). The immunofluorescence showed that CX43 in the sham group was mainly distributed in the intercalated disc between myocardial cells, which were arranged neatly in line. The distribution of CX43 in the model group was disordered and the fluorescence intensity decreased. Compared with the model group, the distribution of CX43 in each drug group improved (Figure 3(b)).

3.4. Effect of WenXin KeLi on the Expression of Autophagy-Related Protein. Compared with the model group, the expression of LC3II/LC3I and Beclin1 protein decreased significantly in each drug group and the expression of P62 protein increased significantly in the WXKL-HD group and metoprolol group (Figure 4).

3.5. Effect of WenXin KeLi on PI3K-AKT-mTOR Autophagy Pathway in Rats with MI. Four weeks after the establishment of the MI model, the protein expression of p-PI3K, AKT, p-AKT (473), p-AKT (308), and p-mTOR in the model group were significantly lower than those in the sham group. Compared with the model group, the expression of AKT, p-PI3K, p-AKT (308), p-AKT (473) and p-mTOR increased significantly after four weeks of treatment with WenXin KeLi and Metoprolol (Figure 5(a)). Four weeks after the operation, the laser confocal results showed that the fluorescence intensity of LC3 in the model group was significantly higher than that in the sham group. Compared with the model group, the fluorescence intensity of LC3 decreased significantly. Compared with the sham group, the fluorescence intensity of CX43 decreased significantly in the model group, while that increased significantly in each drug group. The correlation coefficient between LC3 fluorescence intensity and CX43 fluorescence intensity was -0.79, showing a significant negative correlation (Figure 5(b)).

4. Discussion

MI is an acute and critical condition of coronary heart disease. Due to the blocking of the blood supply to the myocardium of the coronary artery, local necrosis occurs in a part of the myocardium due to severe persistent ischemia. With the expansion of infarct scope, heart failure or arrhythmia will eventually lead to death [2]. Through the experiment of ventricular fibrillation induced by electrical stimulation, we have observed that the VFT decreased significantly in the model group. The VFT is the minimum current intensity of ventricular fibrillation, which can directly reflect the cardiac electrical stability and ventricular

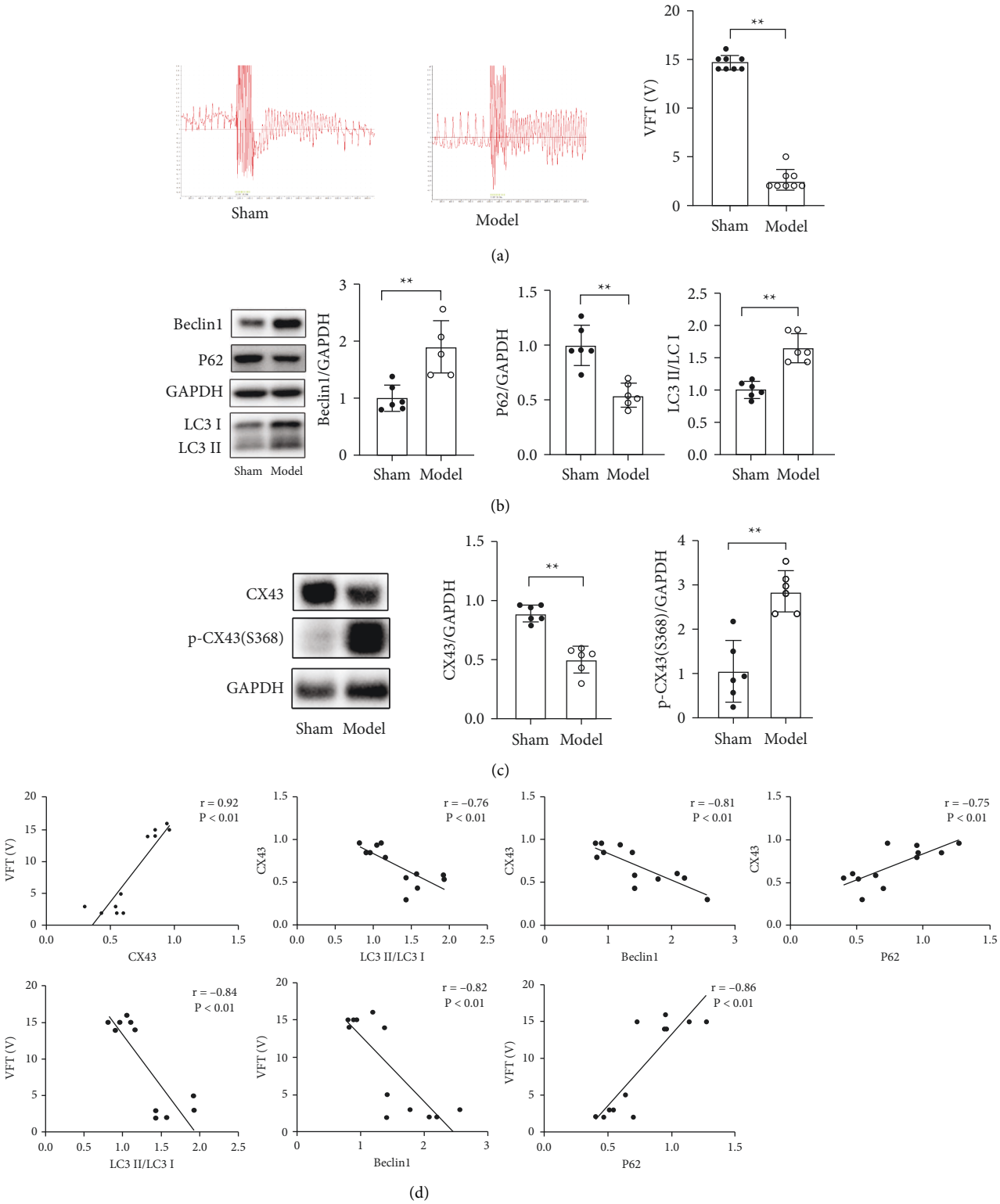

Figure 1: Study on the correlation between cardiac autophagy and arrhythmia in rats with MI: (a) VFT of rats in sham group and model group was measured by electrical stimulation; (b) the expression of autophagy-related proteins in sham group and model group was detected by Western Blot; (c) Western Blot was used to detect CX43 protein expression in sham group and model group; (d) correlation analysis between VFT, CX43, and autophagy in MI rats. Compared with the sham model, $^{**}P < 0.01$.

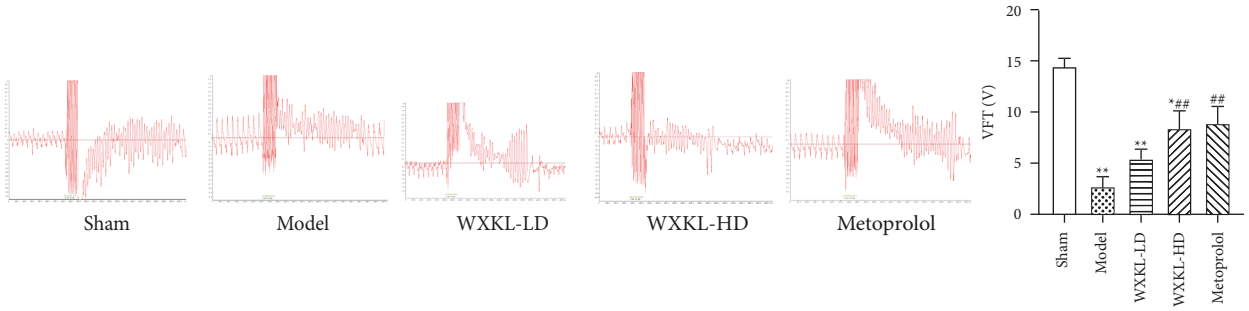

(a)

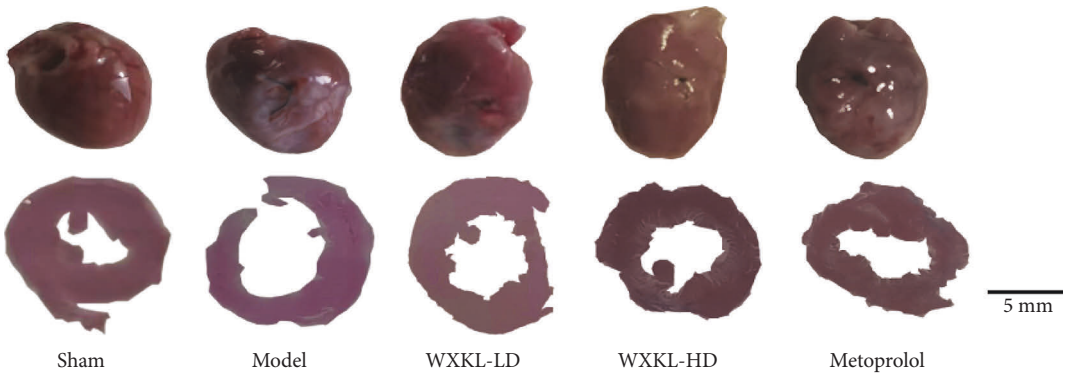

(b)

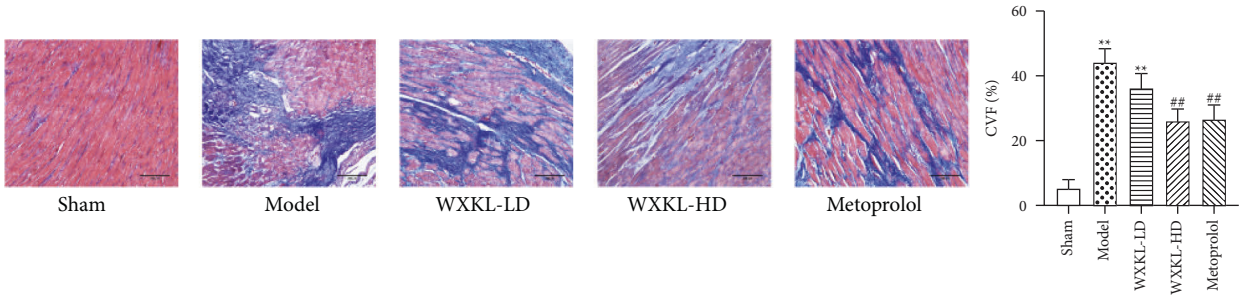

(c)

Figure 2: Continued.

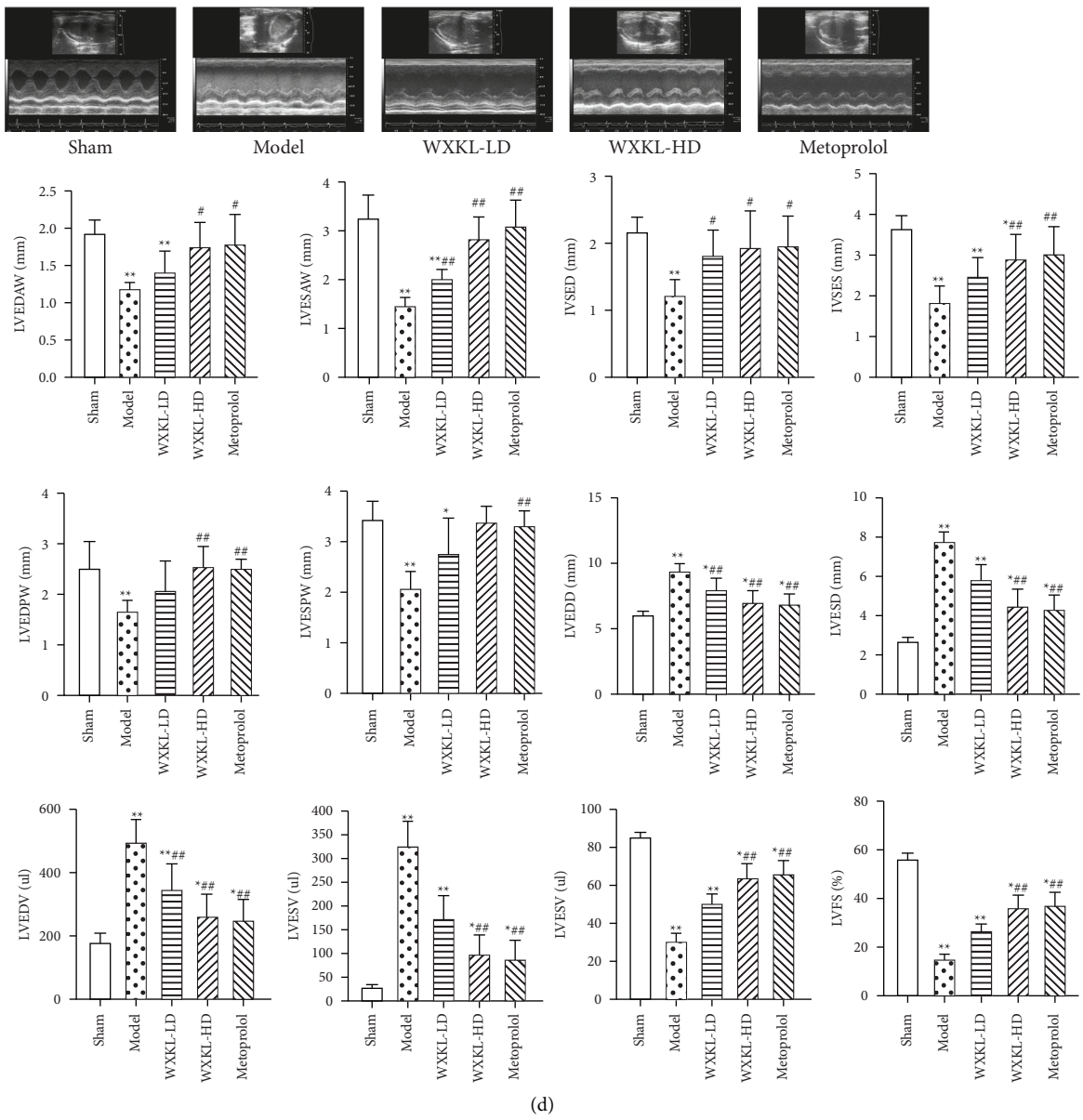

(d)

Figure 2: Effects of WenXin KeLi on arrhythmia and cardiac structure and function in rats with MI. (a) VFT of rats was measured by electrical stimulation; (b) gross and section views of rat hearts; (c) Masson staining was used to determine the CVF of rats; (d) cardiac structural and functional changes were determined by cardiac ultrasound. Compared with the sham group, $^{*}P < 0.05$ and $^{**}P < 0.01$. Compared with the model group, $^{\#}P < 0.05$ and $^{\#\#}P < 0.01$.

fibrillation sensitivity [14]. The decrease of VFT indicates that the sensitivity of infarcted myocardium to arrhythmia is enhanced. Further exploration of the internal mechanism of arrhythmia after MI is of great significance to improve the prognosis and outcome of the disease.

In the heart, connexin is the basis for maintaining normal communication, electrical conduction, and rhythmic contraction between cardiomyocytes [15]. Connexins form a half-channel in the form of the hexamer, and the two half-channels of adjacent cells are docked to form a gap junction channel, which is a transmembrane channel of electrical and chemical coupling between cardiomyocytes [5, 16]. In this experiment, the expression of CX43 decreased and the phosphorylated expression of the Ser368 site of CX43 increased significantly in the model group after MI. The phosphorylation change of the S368 site could lead to the internalization and degradation of connexin, resulting in the closure of the gap junction channel [17]. The distribution of CX43 also changed from the end-to-end junction located at the leap disc to the side-to-side junction parallel to the long axis of cardiac fibers, and the arrangement of CX43 was disordered or even disappeared, resulting in abnormal conduction of impulses and changes in synchronization and coordination of cardiac electrical activity, eventually resulting in arrhythmia. Correlation analysis showed that there was a significant positive correlation between CX43

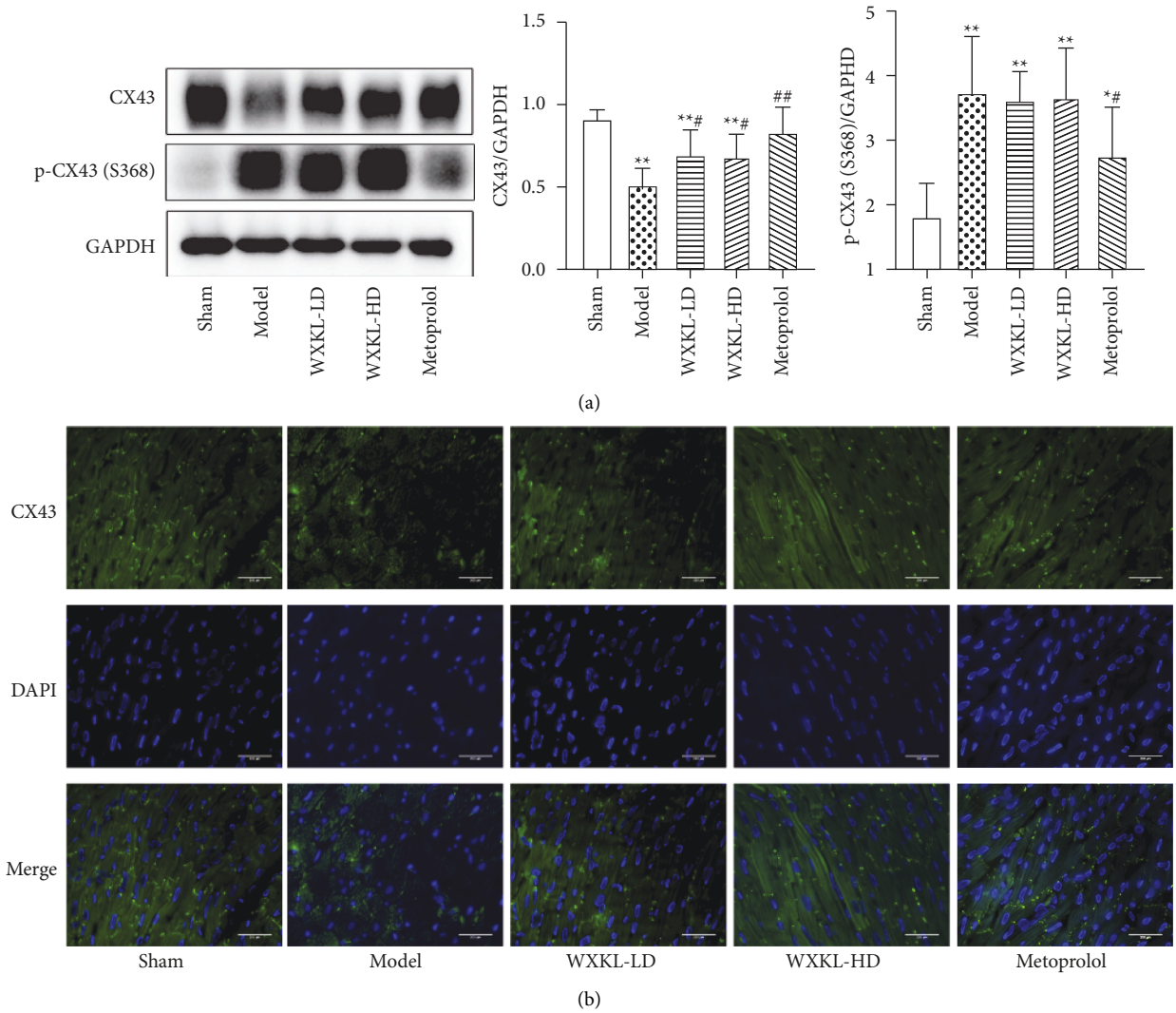

Figure 3: Effect of WenXin KeLi on CX43 protein expression. (a) The expression of CX43 protein in each group was detected by Western Blot; (b) the distribution of CX43 in each group was observed by immunofluorescence. Compared with the sham group, $^{*}P < 0.05$ and $^{**}P < 0.01$. Compared with the model group, $^{\#}P < 0.05$ and $^{\#\#}P < 0.01$.

and VFT after MI, that is, the expression of CX43 decreased, the VFT decreased, and the risk of arrhythmia increased. Since improving the expression of CX43 can effectively reduce the occurrence of arrhythmia after MI [18]. Therefore, further research on the molecular mechanism of regulating connexin could provide ideas for the prognostic treatment of MI.

In recent years, the role of autophagy in cardiovascular diseases has attracted extensive attention [19]. Adaptive autophagy can maintain cell dynamic balance through degradation and recycling of damaged organelles; however, excessive and persistent autophagy can degrade normal organelles and consume energy, thus inducing cell death [3, 4]. Some studies have shown that atrial fibrillation is associated with impaired cardiac autophagy [20], while other studies have shown that autophagy increases in cardiomyocytes of severe mitral regurgitation with atrial fibrillation [21]. Therefore, the relationship between arrhythmia and autophagy after MI still needs further experimental study. Western Blot results showed that the expression of autophagy markers LC3II/LC3 I and Beclin1 were significantly up-regulated and P62 was downregulated in rats with MI. LC3 is an autophagy marker protein. Its C terminal is cleaved by cysteine protease (ATG4B) to form LC3-I. LC3-I combines with phosphatidylethanolamine (PE) to form LC3-II, which participates in the extension of the autophagy membrane and is related to the formation of the autophagosome. Therefore, when the expression of LC3-II increases, autophagy is activated [22]. Beclin1, as a specific autophagy protein, can regulate autophagosome formation. Thus, the significant up-regulation of Beclin1 gene activity indicates autophagy activation [23]. P62, an autophagy substrate protein with multiple domains, binds to LC3 through its C-terminal LC3 interacting region (LIR) and aggregates the protein to be degraded. During the process of protein accumulation, P62 expression increases, but

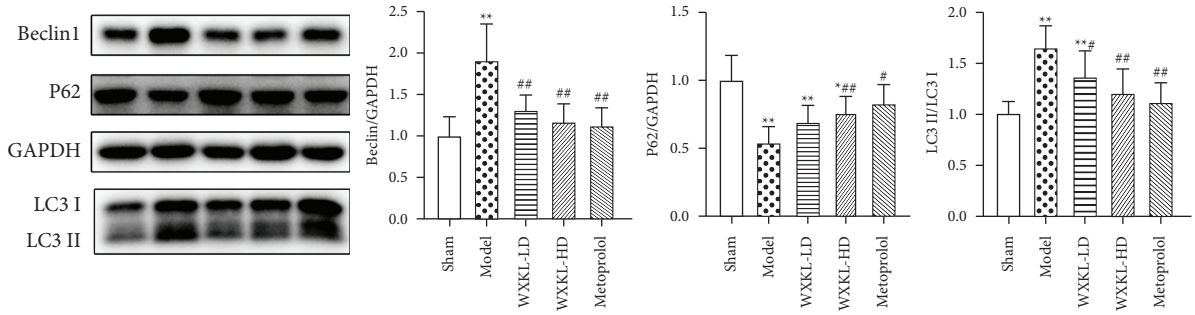

Figure 4: The expression of Beclin1, P62, and LC3II/LC3I protein was detected by Western Blot. Compared with the sham group, $^{*}P < 0.05$ and $^{**}P < 0.01$. Compared with the model group, $^{\#}P < 0.05$ and $^{\#\#}P < 0.01$.

decreases when the autophagy lysosomal maturation degradation reaction begins [24]. Therefore, the above results showed that the level of autophagy of cardiomyocytes in the model group increased after MI.

The results of correlation analysis between autophagy and CX43 showed that there was a significant negative correlation between Beclin1, LC3II/LC3I, and CX43 expression, and a significant positive correlation between P62 and CX43 expression, indicating that the increase of autophagy level after MI was correlated with the increase of CX43 degradation. Autophagy was found to be involved in the degradation of connexin [25]. The internalization and degradation of CX43 in myocardial tissue of dogs with heart failure can be mediated by the autophagolysosomal pathway [6]. The overactivation of autophagy can mediate increased CX43 degradation and induce increased apoptosis in H9c2 cardiomyocytes [26]. The above studies demonstrated the correlation between enhanced autophagy levels and increased CX43 degradation after MI, while increased CX43 degradation can lead to an increased risk of arrhythmia, which further proved that autophagy was associated with arrhythmia after MI. In this study, the correlation analysis between autophagy and VFT after MI showed that there was a significant negative correlation between cardiomyocyte autophagy-related proteins Beclin1, LC3II/LC3I, and VFT, and a significant positive correlation between P62 expression and VFT, suggesting that the overactivation of myocardial autophagy after MI was related to the increased risk of arrhythmia. There was a correlation between enhanced autophagy and arrhythmia. During myocardial ischemia-reperfusion in mice, the expression levels of autophagy markers Beclin1 and LC3II in the model group with ventricular fibrillation were significantly higher than those in the control group without ventricular fibrillation [27]. Inhibiting the level of autophagy can reduce the incidence of arrhythmia in desmosome hereditary heart disease [28]. The above studies further supported the fact that the activation of autophagy increased the risk of arrhythmia in rats with MI. In summary, the above studies showed that the increased risk of arrhythmia after MI was related to the increased degradation of CX43. The abnormal distribution and quantity of CX43 lead to intercellular conduction dysfunction, which can induce arrhythmia. The activation of autophagy was significantly correlated with the increase of CX43 degradation and the risk of ventricular fibrillation, suggesting that the pathological basis of malignant arrhythmia after MI was related to the excessive stress of autophagy and the increase of CX43 degradation.

WenXin KeLi is a TCM preparation for the treatment of arrhythmia in the clinic, which has significant efficacy in alleviating arrhythmia symptoms after MI and improving patients' survival quality [29]. In this experiment, we have observed that compared with the model group, the scope of MI in the WenXin KeLi group was significantly reduced. Masson staining showed that the scope of myocardial fibrosis was significantly reduced, the disordered arrangement of cardiomyocytes was improved, and the pathological changes in the heart were gradually reduced. Ultrasound detection results showed that after WenXin KeLi treatment, the structure and function of the heart were significantly improved, the ventricular wall was thickened, myocardial contractility was enhanced, cardiac ejection fraction and stroke output were increased, and the VFT of rats was significantly higher than that in model group. The results showed that WenXin KeLi could improve the cardiac structure and function of rats after MI, reduced the risk of arrhythmia complications after MI, and played a role in cardiac protection, which laid a foundation for further research on the molecular mechanism of WenXin KeLi in protecting the heart.

However, whether the pharmacological effect of WenXin KeLi on improving the prognosis of MI was related to the regulation of cardiac autophagy level and Cx43 expression still lacks of experimental evidence. This study further investigated the effects of Wenxin KeLi on autophagy and CX43 expression after MI. The Western Blot results showed that compared with the model group, the expression of autophagy positively related proteins Beclin1 and LC3II/LC3I decreased and the expression of autophagy negative regulator P62 increased in the WenXin KeLi group, indicating that Wenxin KeLi could significantly reduce the level of overactivated autophagy after MI. WenXin KeLi can regulate autophagy and inhibit cardiomyocyte hypertrophy induced by angiotensin II [30]. Ginsenoside Rb1 could inhibit cardiomyocyte autophagy and reduce myocardial ischemia-reperfusion injury [31]. Ginsenoside Rb1 was the active chemical component in WenXin KeLi, which further proved the regulatory effect of

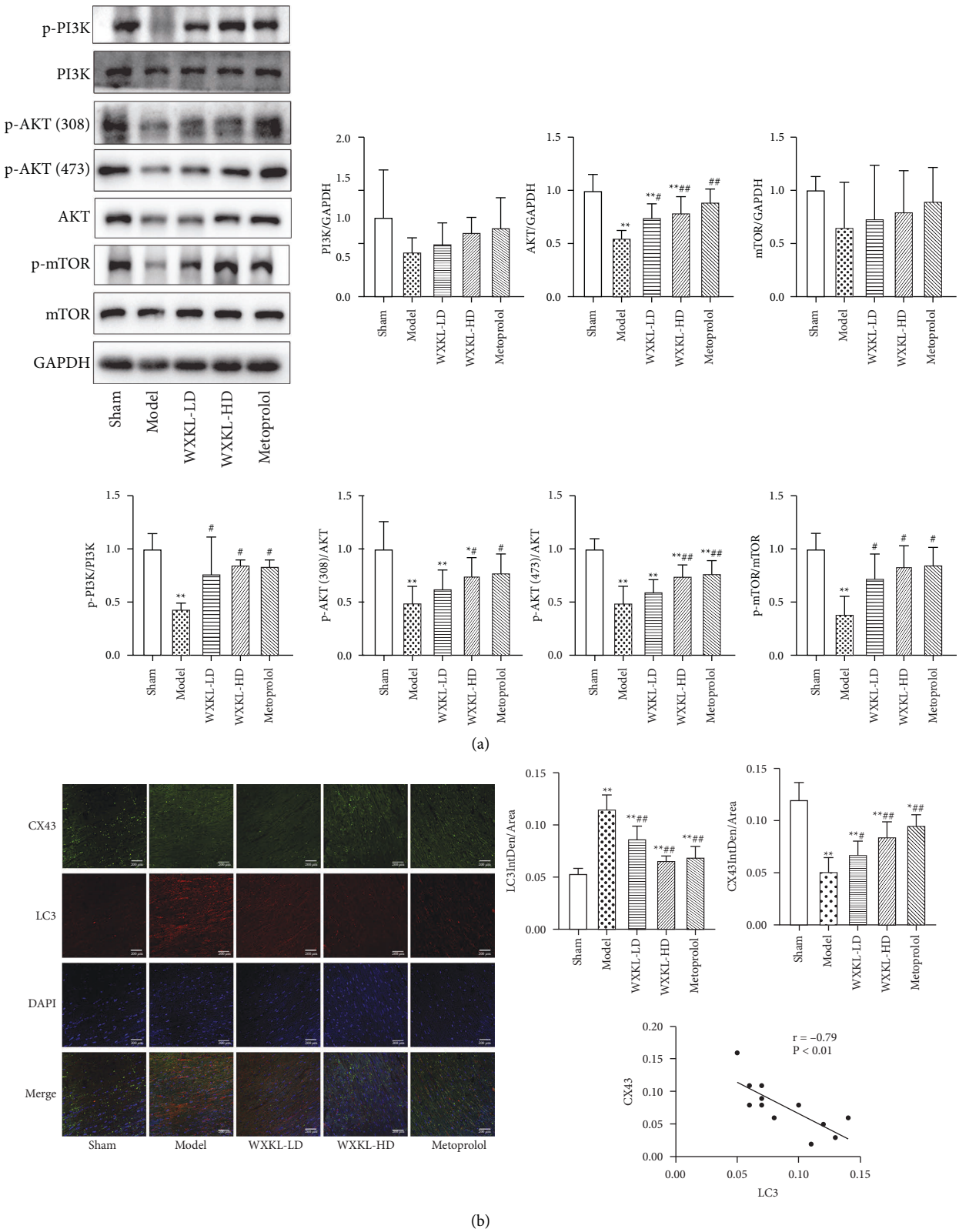

Figure 5: Effect of WenXin KeLi on PI3K-AKT-mTOR autophagy pathway in rats with MI. (a) Protein expression of PI3K-AKT-mTOR pathway in rats of each group was detected by Western Blot; (b) CX43 and LC3 fluorescence intensity were detected by confocal and the correlation analysis of fluorescence intensity between LC3 and CX43. Compared with the sham group, $^{*}P < 0.05$ and $^{**}P < 0.01$. Compared with the model group, $^{\#}P < 0.05$ and $^{\#\#}P < 0.01$.

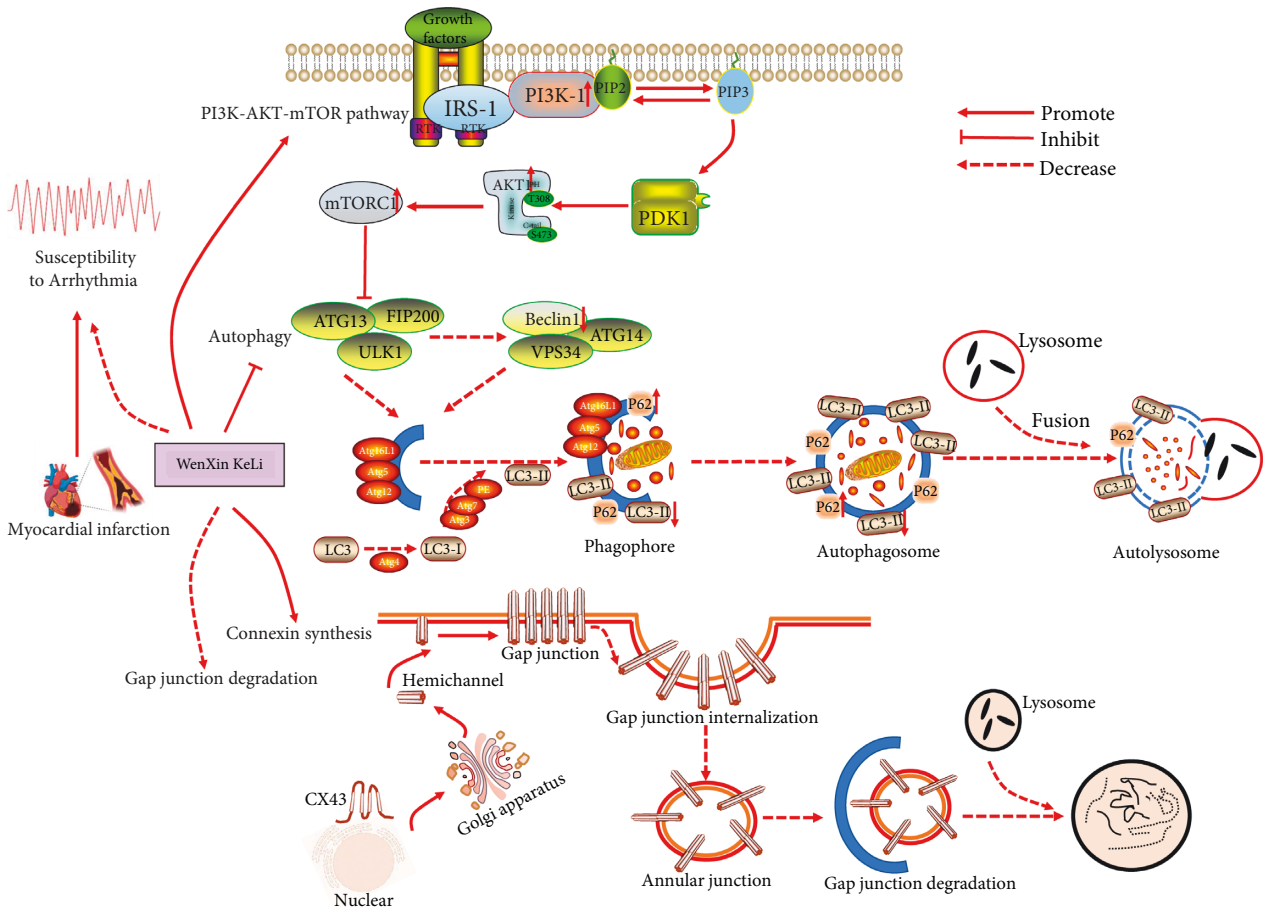

Figure 6: The increased risk of arrhythmia after MI was related to the overactivation of autophagy after MI. WenXin KeLi could activate the PI3K-AKT-mTOR signal pathway, up-regulate the phosphorylation expression of PI3K, AKT, and mTOR proteins, inhibit the level of cardiac autophagy, reduce the expression of Beclin1 and LC3-II proteins, increase the expression of the P62 protein, and reduce the risk of arrhythmia after MI. The increased risk of arrhythmia after MI was related to the decreased expression of CX43 after MI. The internalization and degradation of CX43 increased after MI. WenXin KeLi could significantly increase the expression of CX43, reduce gap junction degradation and reduce the risk of arrhythmia after MI.

WenXin KeLi on the overactivated autophagy level after MI. Our study observed that in the WenXin KeLi group, the expression of CX43 was increased, the distribution was improved, and the communication connection, electrical conduction, and rhythmic contraction between cardiomyocytes gradually recovered, and the pathological changes in cardiac structure and function were improved after MI. WenXin KeLi also could protect MI by improving CX43 expression through miR-1 [32]. The chemical component ginsenoside Rg1, a chemical component in WenXin KeLi, could regulate the biosynthesis and degradation of CX43 [33], indicating that WenXin KeLi could improve the expression and distribution disorder of CX43. The above results showed that 4 weeks after MI, the autophagy of the model group was overactivated, the degradation of CX43 was increased, and the risk of arrhythmia was increased. WenXin KeLi could reduce the overactivated autophagy level, improve the expression of CX43 and play an antiarrhythmic role.

The PI3K-AKT-mTOR signaling pathway is a classical pathway that regulates the autophagy mechanism [10]. PI3K includes three subtypes: type I, II, and III. Type I PI3K activation is an important segment in regulating the mTOR autophagy pathway. AKT is the main downstream target of PI3K. The activation of AKT lies in the phosphorylation of its threonine 308 and serine 473 sites. The activated AKT is transferred to the cytoplasm or nucleus to regulate the downstream target protein mTOR [34]. mTOR, as the main inhibitory signal in the process of autophagy, is positively regulated by the PI3K-AKT pathway [35]. Studies have shown that activation of the PI3K-AKT-mTOR signaling pathway could reduce excessive autophagy and myocardial injury of myocardial cells after ischemia-reperfusion [31]. In this experiment, compared with the sham group, the expression of AKT in MI rats decreased significantly, PI3K, AKT and mTOR dephosphorylated and inactivated, and the expression of LC3II increased significantly. The confocal results showed that there was a significant negative correlation between LC3 and CX43 in the model group, indicating that the PI3K-AKT-mTOR signal pathway was inhibited, autophagy was overactivated, and the expression of connexin was decreased after MI. These alterations

constituted an intrinsic pathological mechanism of the signal transduction disorder between cardiomyocytes and the increased risk of arrhythmia after MI, which aggravated the disease progression after MI. The overall animal research results were consistent with the observation that the PI3K-AKT-mTOR pathway regulated autophagy activity and downregulated CX43 in H9c2 cardiomyocytes [36]. Compared with the model group, after 4 weeks of WenXin KeLi intervention, the PI3K-AKT-mTOR signal pathway was activated and the phosphorylation expression of PI3K, threonine 308, and serine 473 sites of AKT, as well as mTOR, were significantly increased, while the expression of LC3II was reduced, the autophagy overactivation state was inhibited, and CX43 expression was increased. In conclusion, the results indicated that WenXin KeLi could activate the PI3K-AKT-mTOR signal pathway, inhibit excessive autophagy in cardiomyocytes, improve connexin expression and distribution, then improve the prognosis of MI and eventually exert the cardioprotective molecular mechanism.

5. Conclusion

Our study confirmed at the basic experimental level that the increased risk of arrhythmia after MI was closely related to the hyperactivation of autophagy and the decreased expression of CX43 after MI. It revealed that the cardioprotective mechanism of WenXin KeLi in improving cardiac structure and function and reduced the risk of arrhythmia in rats after MI, which was related to the activation of the PI3K- AKT-mTOR signal pathway and the improvement of cardiac autophagy and CX43 expression in rats after MI (Figure 6).

Data Availability

The data used to support the findings of this study are available from the corresponding author upon request.

Conflicts of Interest

The authors declare that they have no conflicts of interest.

Authors' Contributions

Meng Lv, Ding Yang, and Xiaodi Ji contributed equally to this paper.

Acknowledgments

This work was financially supported by the National Natural Science Foundation of China (Grant No. 81673895).

References

[1] Editorial Board of China Cardiovascular Health and Disease Report, "Overview of China cardiovascular health and disease report 2020," *Chinese cardiovascular research*, vol. 19, no. 7, pp. 582–589, 2020.

[2] C.-Y. Li, Y.-G. Li, and T. D. Ruddy, "Cardiac sympathetic nerve sprouting and susceptibility to ventricular arrhythmias after myocardial infarction," *Cardiology Research and Practice*, vol. 2015, Article ID 698368, 8 pages, 2015.

[3] Y.-F. Wu, Q. Mao, and X.-L. Liang, "Targeting the MicroRNA-490-3p-ATG4B-autophagy Axis relieves myocardial injury in ischemia reperfusion," *Journal of Cardiovascular Translational Research*, vol. 14, no. 1, pp. 173–183, 2021.

[4] X. Wen, Y. Yang, and D. J. Klionsky, "Moments in Autophagy and disease: Past and present," *Molecular Aspects of Medicine*, vol. 82, Article ID 100966, 2021.

[5] M. A. Beardslee, J. G. Laing, E. C. Beyer, and J. E. Saffitz, "Rapid turnover of connexin43 in the adult rat heart," *Circulation Research*, vol. 83, no. 6, pp. 629–635, 1998.

[6] G. G. Hesketh, M. H. Shah, V. L. Halperin et al., "Ultrastructure and regulation of lateralized Connexin43 in the failing heart," *Circulation Research*, vol. 106, no. 6, pp. 1153–1163, 2010.

[7] X.-F. Li, G. Tian, L. Xu et al., "Wenxin Keli for the Treatment of Arrhythmia-Systems Pharmacology and In Vivo Pharmacological Assessment," *Front Pharmacol*, vol. 12, Article ID 704622, 2021.

[8] X.-Y. Wang, Y. Wang, X. Y. Feng et al., "Systematic review and meta-analysis of randomized controlled trials on Wenxin keli," *Drug Design, Development and Therapy*, vol. 10, pp. 3725–3736, 2016.

[9] S.-Q. Shi, Y.-G. Chu, Q.-L. Jia, and Y. Hu, "Comparative efficacy and safety of wenxin granule combined with antiarrhythmic drugs for atrial fibrillation: a protocol for a systematic review and network meta-analysis," *Medicine*, vol. 100, no. 3, Article ID e24434, 2021.

[10] Z.-R. Xu, X. Han, D.-M. Ou et al., "Targeting PI3K/AKT/mTOR-mediated autophagy for tumor therapy," *Applied Microbiology and Biotechnology*, vol. 104, no. 2, pp. 575–587, 2020.

[11] W.-H. Yang, T. Guo, and L. Yang, "Establishment of acute myocardial infarction model in rats," *Chinese Journal of Gerontology*, vol. 21, no. 35, pp. 6019–6021, 2015.

[12] L. Wang, M.-J. Zhao, and T. Yang, "To study the early evaluation and screening method of heart failure model after myocardial infarction from the correlation analysis of ECG and echocardiography," *Journal of Integrated Traditional Chinese and Western*, vol. 15, no. 22, pp. 2816–2820, 2017.

[13] J.-H. Huang and X.-H. Huang, "Equivalent dose conversion between animals and between animals and human body in pharmacological test," *Chinese Journal of Clinical Pharmacology and Therapeutics*, vol. 9, no. 9, pp. 1069–1072, 2004.

[14] N. Trevisi, J. Silberbauer, A. Radinovic et al., "New diagnostic criteria for identifying left-sided ventricular ectopy using noncontact mapping and virtual unipolar electrogram analysis," *Europace*, vol. 17, no. 1, pp. 108–116, 2015.

[15] P. Michela, V. Velia, P. Aldo, and P. Ada, "Role of connexin 43 in cardiovascular diseases," *European Journal of Pharmacology*, vol. 768, no. 2015, pp. 71–76, 2015.

[16] K. Boengler and R. Schulz, "Connexins in cardiac ischemia," *Current Opinion in Physiology*, vol. 2, pp. 123–128, 2018.

[17] P. D. Lampe, E. M. Tenbroek, J. M. Burt, W. E. Kurata, R. G. Johnson, and A. F. Lau, "Phosphorylation of Connexin43 on serine368 by protein kinase C regulates gap junctional communication," *Journal of Cell Biology*, vol. 149, no. 7, pp. 1503–1512, 2000.

[18] T. Wu, D. Wu, Q.-H. Wu et al., "Effect and mechanism of Irbesartan on occurrence of ventricular arrhythmias in rats with myocardial ischemia through connexin43 (cx43)," *Asian Pacific Journal of Tropical Medicine*, vol. 9, no. 10, pp. 1007–1012, 2016.

[19] A. Nemchenko, M. Chiong, A. Turer, S. Lavandero, and J. A. Hill, "Autophagy as a therapeutic target in cardiovascular disease," *Journal of Molecular and Cellular Cardiology*, vol. 51, no. 4, pp. 584–593, 2011.

[20] L. Garcia, H. E. Verdejo, J. Kuzmicic et al., "Impaired cardiac autophagy in patients developing postoperative atrial fibrillation," *The Journal of Thoracic and Cardiovascular Surgery*, vol. 143, no. 2, pp. 451–459, 2012.

[21] M.-C. Chen, J.-P. Chang, Y.-H. Wang, W. H. Liu, W. C. Ho, and H. W. Chang, "Autophagy as a mechanism for myolysis of cardiomyocytes in mitral regurgitation," *European Journal of Clinical Investigation*, vol. 41, no. 3, pp. 299–307, 2011.

[22] J. I. Satoh, N. Motohashi, Y. Kino et al., "LC3, an autophagosome marker, is expressed on oligodendrocytes in Nasu-Hakola disease brains," *Orphanet Journal of Rare Diseases*, vol. 68, no. 9, p. 11, 2014.

[23] K. J. Schmitz, C. Ademi, S. Bertram, K. W. Schmid, and H. A. Baba, "Prognostic relevance of autophagy-related markers LC3, P62/sequestosome 1, Beclin-1 and ULK1 in colorectal cancer patients with respect to KRAS mutational status," *World Journal of Surgical Oncology*, vol. 14, no. 1, p. 189, 2016.

[24] F. Lin, Y.-T. Zhu, and Z.-H. Qin, "Biomarkers of autophagy," *Advances in Experimental Medicine & Biology*, vol. 12, no. 8, pp. 265–287, 2021.

[25] J. Iyyathurai, J. P. Decuypere, L. Leybaert, C. D'hondt, and G. Bultynck, "Connexins: substrates and regulators of autophagy," *BMC Cell Biology*, vol. 17, no. 1, p. 20, 2016.

[26] C. Li, L. Shi, C. Peng, G. Yu, Y. Zhang, and Z. Du, "Lead-induced cardiomyocytes apoptosis by inhibiting gap junction intercellular communication via autophagy activation," *Chemico-Biological Interactions*, vol. 337, Article ID 109331, 2021.

[27] G. Meyer, A. Czompa, C. Reboul et al., "The cellular autophagy markers beclin-1 and LC3B-II are increased during reperfusion in fibrillated mouse hearts," *Current Pharmaceutical Design*, vol. 19, no. 39, pp. 6912–6918, 2013.

[28] J. Wang, J. Pellman, R. Lyon et al., "SNAP29 restricts cardiac arrhythmias by insulating A subset of desmosomal proteins and Connexin43 from autophagic degradation," *The FASEB Journal*, vol. 35, no. 1, Article ID 02621, 2021.

[29] W. Hua, R.-L. Gao, B.-C. Zhao et al., "The efficacy and safety of wenxin keli in patients with frequent premature ventricular contractions: a randomized, double-blind, placebo-controlled, parallel-group, multicenter trial," *Chinese Medical Journal*, vol. 128, no. 19, pp. 2557–2564, 2015.

[30] J. Li, Y. Li, Y. Zhang, Y. Gao, H. Shang, and Y. Xing, "The inhibitory effect of WenxinKeli on H9C2 cardiomyocytes hypertrophy induced by angiotensin II through regulating autophagy activity," *Oxidative Medicine and Cellular Longevity*, vol. 2017, Article ID 7042872, 11 pages, 2017.

[31] G.-W. Qin, P. Lu, L. Peng, and W. Jiang, "Ginsenoside Rb1 inhibits cardiomyocyte autophagy via PI3K/AKT/mTOR signaling pathway and reduces myocardial ischemia/reperfusion injury," *The American Journal of Chinese Medicine*, vol. 49, no. 08, pp. 1913–1927, 2021.

[32] A.-M. Wu, M.-J. Zhao, L.-X. Lou et al., "Effect of wenxin granules on gap junction and MiR-1 in rats with myocardial infarction," *BioMed Research International*, vol. 2017, Article ID 3495021, 12 pages, 2017.

[33] H.-Q. Wang, S.-W. Yang, Y. Gao et al., "Novel antidepressant mechanism of ginsenoside Rg1: regulating biosynthesis and degradation of connexin43," *Journal of Ethnopharmacology*, vol. 278, Article ID 114212, 2021.

[34] N. D. Pradip and B. L. Jones, *PI3K-mTOR in Cancer and Cancer Therapy*, Springer Nature, New York, NY, USA, 2016.

[35] Q.-W. Fan and W. A. Weiss, "Inhibition of PI3K-AKT-mTOR signaling in glioblastoma by mTORC1/2 inhibitors," *Methods in Molecular Biology*, vol. 821, pp. 349–359, 2012.

[36] Y.-G. Bi, G.-Y. Wang, X.-D. Liu, M. Wei, and Q. Zhang, "Low-after-high glucose down-regulated CX43 in H9c2 cells by autophagy activation via cross-regulation by the PI3K/AKT/mTOR and MEK/ERK1/2 signal pathways," *Endocrine*, vol. 56, no. 2, pp. 336–345, 2017.

Hindawi
Evidence-Based Complementary and Alternative Medicine
Volume 2022, Article ID 6539675, 9 pages
https://doi.org/10.1155/2022/6539675

Research Article

The Pseudotargeted Metabolomics Study on the Toxicity of Fuzi Using Ultraperformance Liquid Chromatography Tandem Mass Spectrometry

Huifei Wu,[1] **Wenxia Zhang**,[1] **Hui Lin**,[1] **Qiuming Ye**,[1] **Jiayin Guo**,[2] **and Shijian Quan**[3]

[1]*Zhongshan Hospital of Traditional Chinese Medicine, Zhongshan 528400, China*
[2]*Guangdong Provincial Key Laboratory of Drug Screening, School of Pharmaceutical Sciences, Southern Medical University, Guangzhou 510515, China*
[3]*Guangzhou University of Chinese Medicine, Guangzhou 510006, China*

Correspondence should be addressed to Jiayin Guo; g1227@smu.edu.cn and Shijian Quan; quansj@gzucm.edu.cn

Received 6 March 2022; Revised 17 July 2022; Accepted 2 August 2022; Published 13 September 2022

Academic Editor: Anca Nicoleta Sutan

Fuzi is commonly used in traditional Chinese medicine. Clinical Fuzi poisoning cases have frequently been reported. Glycyrrhizae Radix is often used to alleviate Fuzi's toxicity. However, the poisoning mechanism of Fuzi and the detoxication mechanism of Glycyrrhizae Radix are still not clear. We identified the chemical components of Fuzi at different decoction times (0.5, 1, 2, 4, and 6 h) using ultrahigh performance liquid chromatography quadrupole time-of-flight mass spectrometry. A total of 35 compounds were detected in the Fuzi decoction, including diester alkaloids, monoester alkaloids, amino acids, phenolic acids, organic acids, glycosides, and sugars among others. The content of diester alkaloids (i.e., subaconitine, neoaconitine, and aconitine) in the Fuzi decoction decreased after 2 h of decoction time, while the content of monoester alkaloids (i.e., benzoyl aconitine and benzoyl subaconitine) reached a peak at 2 h. A total of 32 rats were randomly divided into four groups, including 8 cases in the low-dosage Fuzi decoction group A, 8 cases in the high-dosage Fuzi decoction group B, 8 cases in the Fuzi and glycyrrhizae decoction group C, and 8 cases in the control group D. The decoction was administered orally for 7 days. Then, a serum was obtained. The metabolites' changes were analyzed in serum metabolomics using liquid chromatography-tandem mass spectrometry (UPLC-MS/MS). Statistical analysis and pathway analysis were used to assess the effects of glycyrrhizae on the metabolic changes induced by Fuzi. The behavioral and biochemical characteristics indicated that Fuzi exhibited toxic effects on rats and their metabolic profiles changed. However, the metabolic profiles of the glycyrrhizae group became similar to those of the control group. These profiles showed that glycyrrhizae can effectively improve Fuzi poisoning rats. Our study demonstrated that the established pseudotargeted metabolomics is a powerful approach for investigating the mechanisms of herbal toxicity.

1. Introduction

Traditional Chinese medicine is generally considered natural and harmless [1–3]. *Aconitum carmichaelii* (called Fuzi in Chinese) has positive pharmacological effects on various diseases such as painful joints, collapse, rheumatic fever, bronchial asthma, syncope, edema, various tumors, and diarrhea [4–6]. Fuzi was first recorded in Shennong's *Materia Medica*. However, its medicinal application on a large scope was limited due to the high toxicity risk and narrow therapeutic range [7]. It is important to establish a standardized chemical method that ensures its safe use. The previous reports demonstrated that aconitine, hypaconitine, and neoaconitine were the main toxic components in Fuzi [8–10]. Therefore, the strategy of reducing toxicity and increasing efficiency was developed to meet the needs of clinical applications. There are a variety of chemical components in Fuzi, so we need to understand how to reduce the content of the toxic ingredients and increase the content of active ingredients.

A clear understanding of the mechanism of Fuzi at the selected decoction time is essential to evaluate its safety. Metabolomics is a comprehensive method for diagnosing diseases, discovering biomarkers, and identifying perturbed pathways [11–14]. Sui et al. investigated the mechanism of aconitine's potential neurotoxicity and nephrotoxicity using a UPLC-Q-TOF-based rat serum and urine metabolomics strategy [8]. Shen et al. evaluated the enhancement of the Glycyrrhizae Radix for the hepatic metabolism of hypaconitine using rat liver S9 [15]. Sun et al. developed an NMR-based metabolomics study of the effect of Glycyrrhizae Radix on the attenuation of toxicity in rats induced by Fuzi [16]. In another previous study, nontargeted metabolomics was applied, but it has the weakness of low sensitivity and poor reproducibility [17]. Targeted metabolomics has the advantage of high sensitivity and good reproducibility. However, it has the weakness of low coverage. Therefore, pseudotargeted metabolomics is a promising tool for the high throughput elucidation of metabolic phenotypes [18].

First, nontargeted serum metabolites were used in full scan and data-dependent modes to generate as high of coverage serum metabolite profiling as possible. Secondly, serum metabolite ion pairs were constructed based on the characteristic fragmental ions and corresponding parent ions of the serum metabolites, which were monitored in an MRM mode in the pseudotargeted metabolomics method. This method combines the advantages of nontargeted and targeted metabolomic approaches.

In a previous study, Luo et al. displayed the dynamic variation patterns of the Aconitum alkaloids in Fuzi during the decoction process [7]. However, there have been few comprehensive identifications of Fuzi components at different decoction times, as well as high sensitivity evaluation methods of the toxic mechanism and detoxification mechanism of Glycyrrhizae Radix.

In our study, we explored the relationship between the chemical components of Fuzi with the decoction time to identify the appropriate decoction time using ultrahigh performance liquid chromatography quadrupole time-of-flight mass spectrometry (UPLC-QTOF). Pseudotargeted rat serum metabolomics was used to evaluate the toxic mechanism of Fuzi and the detoxification mechanism of Glycyrrhizae Radix. This study was the first time where Fuzi poisoning was systematically interpreted, thus providing some information for the future clinical use of Fuzi.

2. Materials and Methods

2.1. Chemicals. HPLC-grade acetonitrile (purity: 99.9%) was supplied by Fisher Scientific (Fair Lawn, NJ, USA). Water was obtained from Watsons. HPLC-grade formic acid (purity: 98%), chloramphenicol (purity: 98%), and clenbuterol (purity: 98%) were purchased from Sigma-Aldrich (St. Louis, MO, USA). Fuzi and Glycyrrhizae Radix were obtained from the Hospital of Traditional Chinese Medicine of Zhongshan (Guangdong, China) and authenticated by Director Wu from the same hospital.

2.2. Preparation of the Decoctions. Fuzi (60 g) was immersed in 200 mL water for 30 min and was then boiled for 0.5, 1, 2, 4, and 6 h, respectively. The supernatant was collected by filtration and centrifuged for 15 min at 4000 g. It was then concentrated to a final volume of 20 mL. The preparation of the Glycyrrhizae Radix decoction was the same as that for Fuzi. Glycyrrhizae decoction containing 3 g raw material per mL was obtained.

2.3. Animal Experiment. Thirty-two male Wistar rats (180–220 g) were supplied by the Southern Medical University Laboratory Animal Center and were allowed to acclimatize in cages for 1 week before the experiment. The rats were randomly divided into four groups ($n = 8$/group) as follows: oral gavage with Fuzi at a dose of 30 g/kg (group A), oral gavage with Fuzi at a dose of 60 g/kg (group B), oral gavage with Fuzi and glycyrrhizae at a dose of 60 g/kg (group C), and oral gavage of the same volume of water to healthy controls (group D) as the other three groups. All the groups were given intragastric administrations twice a day for 7 days.

2.4. Collection and Preparation of Serum Samples. Serum samples were collected from the retro-orbital venous plexus 7 days after administration. Then, 300 μL acetonitrile was added into 100 μL serum and vortex-mixed for about 5 min for protein precipitation. The mixture was centrifuged at 14000 g for 15 min. Finally, 5 μL aliquots of the supernatant were used for analysis.

2.5. Chromatography and Mass Spectrometry

2.5.1. Fuzi Decoction Analysis. Chromatography separation of Fuzi decoction was performed on a Waters T3 column (2.1 mm * 100 mm, 1.8 μm) using a SCIEX ExionLC AD UPLC system (CA, USA). The column temperature was maintained at 40°C, and the mobile phase consisted of 0.1% formic acid in water (Phase A) and acetonitrile (Phase B) at a constant flow rate of 0.3 mL/min. The injection volume was 5 μL. The 45 min binary gradient elution conditions were optimized as follows: linear gradient from 5% to 10% B (0.5–5 min), 10% to 95% B (5–35 min), 95% to 5% B (40-40.1 min), and then the column was returned to its starting conditions of 5% B for 5 min to allow for column re-equilibration. SCIEX X500R QTOF mass spectrometry (CA, USA) was used to analyze the components of the Fuzi decoction. The optimized MS conditions were as follows: TOF MS scan range: m/z 70–1500; TOF MS/MS scan range: m/z 50–1500; curtain gas: 35 psi; nebulizer gas: 55 psi; heater gas: 50 psi; temperature: 550°C; ion spray voltage: 5500 V (positive mode)/−4500 V (negative mode); declustering potential: 100 V (positive mode)/−100 V (negative mode); collision potential: 40 ± 20 eV (positive mode)/−40 ± 20 eV (negative mode). A typical information-dependent acquisition (IDA) process was used to carry out the MS/MS experiment.

2.5.2. Pseudotargeted Metabolomics Analysis. Chromatography separation of serum samples was performed on a Waters C18 BEH column (2.1 mm * 100 mm,

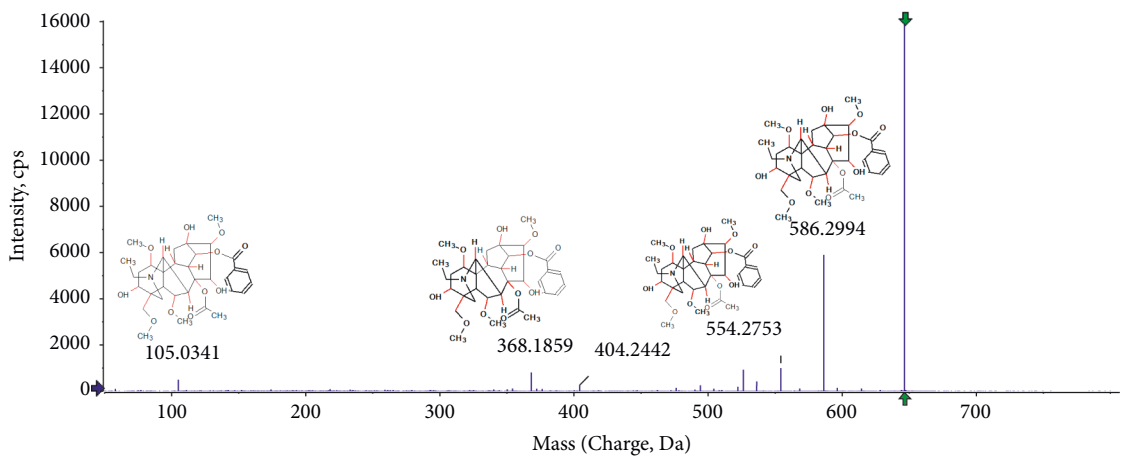

Figure 1: The fragmentation pattern of aconitine.

1.7 μm) using a SCIEX ExionLC AD UPLC system (CA, USA). The column temperature was maintained at 40°C, and the mobile phase consisted of 0.1% formic acid in water (Phase A) and acetonitrile (Phase B) at a constant flow rate of 0.4 mL/min. The injection volume was 10 μL. The 11 min binary gradient elution conditions were optimized as follows: linear gradient from 5% to 95% B (1–7 min), 95% to 5% B (9.5-9.6 min), and then the column was returned to its starting conditions of 5% B for 1.5 min to allow for column re-equilibration. SCIEX 4000 QTrap mass spectrometry (CA, USA) was used to detect the metabolites of serum samples. The optimized MS conditions were as follows: curtain gas: 35 psi; nebulizer gas: 55 psi; heater gas: 50 psi; temperature: 550°C; ion spray voltage: 5500 V (positive mode)/−4500 V (negative mode). The MRM transitions of 166 metabolites are shown in the Supplementary Materials (MRMs), which include the metabolite name, their parent ions (Q1), and product ions (Q3).

2.6. Data Processing and Statistical Analysis. The components of Fuzi were identified by searching the SCIEX commercialization database using SCIEX OS software. The serum samples were analyzed using MultiQuant 3.0.3 software (CA, USA). Multivariate statistical analysis was performed on MetaboAnalyst 4.0 (Xia Lab at McGill University, Montreal, QC, Canada). Partial least-squares discriminant analysis (PLS-DA) was used to model all features of the four groups. All the metabolites with a significance threshold that satisfies the corrected p value cut-off of 0.05 in one-way ANOVA were considered as potential biomarkers.

3. Results

3.1. Identification of Fuzi Components. All components of Fuzi were represented as chromatographic peaks. The parent ions and their product ions were obtained for structural identification. To illustrate the identification of components, we took the m/z 646.3233 ($t_R = 20.72$ min) as an example to be described as follows. Its molecular formula was speculated to be $C_{34}H_{47}NO_{11}$ based on its parent ion and isotope abundance. In the positive mode, its product ions were observed at m/z 586.2994, 554.2753, 368.1859, and 105.0341, which could be obtained by neutral loss of $-C_2H_4O_2$, $-C_3H_8O_3$, $-C_{14}H_{32}O_5$, and $-C_{27}H_{43}NO_{10}$, respectively. Finally, according to the SCIEX Commercialize Traditional Chinese Medicine database, the ion was tentatively identified as aconitine. The fragmentation pattern of aconitine is shown in Figure 1. The components of Fuzi decoction were identified and are listed in Table 1.

3.2. The Comparison of Fuzi Components at Different Decoction times. The Fuzi decoction times were 0.5, 1, 2, 4, and 6 h, respectively. The content of the components was compared at different decoction times, as can be seen in Table 2. Hypaconitine, mesaconitine, and aconitine are diester alkaloids with strong toxicity. In our study, their content increased from 0 h to 1 h of decoction time and decreased after 2 h of decoction time. The results showed that diester alkaloids were thermally unstable. The content of benzoylhypacoitine, benzoylmesaconine, hydroxypurine, adenine, adenosine, and ferulic acid increased from 0.5 h to 2 h of decoction time and decreased after 2 h of decoction time. The content of neoandrographolide, p-coumaric acid, trigonelline, higenamine, and tuberostemonine increased from 0.5 to 1 h of decoction time. Phenprobamate, leucine, L(+)-arginine, L-valine, L-tryptophan, caffeic acid, vanillic acid, citric acid, amber acid, succinic acid, L-malic acid, salidroside, salidroside, guanosine, maltopentaose, D-galactose, D-(+)-mannose, nicotinic acid, 6-methyl coumarin, neoandrographolide, methyl 4-hydroxybenzoate, and norcantharidin can all be detected at the decoction time of 2 h. Therefore, the Fuzi decoction at 2 h was used for the metabolomics study.

3.3. Multivariate Statistical Analysis. Serum samples were divided into the following four groups: group A (30 g/kg dosage of Fuzi), group B (60 g/kg dosage of Fuzi), group C (60 g/kg dosage of Fuzi and 60 g/kg dosage of glycyrrhizae), and group D (control). The multireaction monitor (MRM) trigger enhanced product ion mode was applied to detect the serum metabolites. Typical serum chromatograms are shown in Figure 2. Chromatographic peaks of metabolites

Table 1: The identified components of Fuzi.

N.O.	RT (min)	Components	Formula	Ionization	Parent ion (*m/z*)	Mass error (ppm)	Product ions (*m/z*)
1	0.87	L (+)-arginine	$C_6H_{14}N_4O_2$	$[M+H]^+$	175.1185	−2.8	130.0981; 116.0708; 70.0645; 60.0558
2	0.90	D-galactose	$C_6H_{12}O_6$	$[M-H]^-$	179.0565	2.4	89.0309; 71.0209; 59.0188
3	0.90	D-(+)-mannose	$C_6H_{12}O_6$	$[M-H]^-$	179.0563	0.8	89.0319; 71.0190; 59.0193
4	0.99	Trigonelline	$C_7H_7NO_2$	$[M+H]^+$	138.0549	−0.5	94.0661; 92.0501; 78.0345; 65.0395; 51.0225
5	1.02	L-malic acid	$C_4H_6O_5$	$[M-H]^-$	133.0146	3.0	115.0136; 89.0322; 72.9996; 71.0200
6	1.09	L-valine	$C_5H_{11}NO_2$	$[M+H]^+$	118.0864	1.5	72.0816; 57.0560; 55.0553
7	1.28	Maltopentaose	$C_{30}H_{52}O_{26}$	$[M-H]^-$	827.2687	1.6	665.2686; 587.2333; 545.2182; 425.1672; 341.1378; 281.1107; 179.0731; 161.0594; 101.0324
8	1.33	Adenine	$C_5H_5N_5$	$[M+H]^+$	136.0614	−2.6	119.0364; 109.0517; 92.0253; 65.0142; 66.0219
9	1.33	Citric acid	$C_6H_8O_7$	$[M-H]^-$	191.0196	−0.7	129.0300; 111.0173; 87.0155; 85.0365; 67.0242; 57.0394
10	1.35	Nicotinic acid	$C_6H_5NO_2$	$[M+H]^+$	124.0397	2.9	80.0514; 78.0343; 53.0395; 51.0219
11	1.59	6-hydroxypurine	$C_5H_4N_4O$	$[M+H]^+$	137.0457	−0.6	119.0362; 110.0358; 94.0406; 82.0416; 65.0141; 55.0300
12	1.62	Leucine	$C_6H_{13}NO_2$	$[M+H]^+$	132.1021	1.3	86.0968; 72.9396; 56.0489
13	1.65	Amber acid	$C_4H_6O_4$	$[M-H]^-$	117.0194	0.3	99.9335; 73.0359; 55.0237
14	1.66	Isoleucine	$C_6H_{13}NO_2$	$[M+H]^+$	132.1022	2.1	86.0967; 69.0726
15	2.32	Adenosine	$C_{10}H_{13}N_5O_4$	$[M+H]^+$	268.1033	−2.9	136.0619; 119.0361
16	2.38	Guanosine	$C_{10}H_{13}N_5O_5$	$[M-H]^-$	282.0844	−0.1	150.0548; 133.0265; 108.0301; 80.0314
17	2.97	Phenprobamate	$C_9H_{11}NO_2$	$[M+H]^+$	166.0863	0.0	120.0809; 103.0544; 91.0548; 77.0388; 51.0231
18	3.78	Tuberostemonine	$C_{22}H_{33}NO_4$	$[M+H]^+$	376.2479	−0.9	300.1972; 136.0601
19	5.84	L-tryptophan	$C_{11}H_{12}N_2O_2$	$[M-H]^-$	203.0827	0.6	142.0802; 116.0611; 74.0317
20	7.52	Salidroside	$C_{14}H_{20}O_7$	$[M-H]^-$	299.1144	2.7	119.0606; 89.0309; 71.0222; 59.0188
21	7.62	Salidroside + NH3	$C_{14}H_{20}O_7{\cdot}NH_3$	$[M+H]^+$	318.1555	2.4	205.0856; 187.0767; 145.0519; 127.0390; 121.0655; 85.0292
22	7.93	Methyl 4-hydroxybenzoate	$C_8H_8O_3$	$[M-H]^-$	151.0407	3.9	136.0393; 92.0335
23	8.00	p-coumaric acid	$C_9H_8O_3$	$[M-H]^-$	163.0400	−0.3	119.0599; 93.0419
24	8.15	Vanillic acid	$C_8H_8O_4$	$[M-H]^-$	167.0352	1.1	152.0238; 108.0306; 91.0261; 65.0075
25	8.17	Norcantharidin	$C_8H_8O_4$	$[M-H]^-$	167.0354	2.2	152.0263; 108.0310; 91.0250
26	8.21	Higenamine	$C_{16}H_{17}NO_3$	$[M+H]^+$	272.1283	0.5	255.1037; 237.0896; 194.0716; 161.0605; 115.0536; 107.0498
27	8.41	6-methylcoumarin	$C_{10}H_8O_2$	$[M+H]^+$	161.0596	−0.9	115.0559; 89.0378; 79.0554; 51.0240
28	9.00	Caffeic acid	$C_9H_8O_4$	$[M-H]^-$	179.0353	2.0	135.0572
29	9.40	Ferulic acid	$C_{10}H_{10}O_4$	$[M+H]^+$	195.0657	2.5	145.0283; 134.0369; 117.0342; 89.0389; 78.0470; 63.0236
30	15.63	Benzoylmesaconine	$C_{31}H_{43}NO_{10}$	$[M+H]^+$	590.2950	−1.7	540.2556; 508.2307; 105.0328
31	17.36	Benzoylhypacoitine	$C_{31}H_{43}NO_9$	$[M+H]^+$	574.3003	−1.4	542.2727; 510.2492; 105.0335
32	18.58	Neoandrographolide + HCOOH	$C_{26}H_{40}O_8{\cdot}HCOOH$	$[M-H]^-$	525.2705	0.0	479.2983; 161.0609; 101.0329
33	19.28	Mesaconitine	$C_{33}H_{45}NO_{11}$	$[M+H]^+$	632.3059	−1.0	572.2820; 540.2582; 354.1692; 105.0334
34	20.67	Hypaconitine	$C_{33}H_{45}NO_{10}$	$[M+H]^+$	616.3106	−1.6	556.2872; 524.2615; 492.2377; 338.1737; 105.0335
35	20.72	Aconitine	$C_{34}H_{47}NO_{11}$	$[M+H]^+$	646.3233	1.7	586.2994; 554.2753; 368.1859; 105.0341

Table 2: The comparison of Fuzi components at different decoction times.

Sample name	0.5 h	1 h	2 h	4 h	6 h
L(+)-arginine	4224486	6052934	6016773	5458557	4017949
D-galactose	171450	220332	248957	240805	186396
D-(+)-mannose	172431	221452	251645	241490	187498
Trigonelline	913625	1381259	1327159	1090388	660688
L-malic acid	6215	191516	91834	75902	1295
L-valine	72167	73913	85500	94464	181698
Maltopentaose	49923	81807	84371	87473	63982
Adenine	938595	1548668	482508	3005214	28002
Citric acid	788565	1697871	1716444	1421501	783274
Nicotinic acid	19520	68645	35373	49658	48757
6-hydroxypurine	1187035	779049	1196645	173327	19006
Leucine	220014	268314	91526	575355	3036
Amber acid	337516	227553	212178	194989	4811
Isoleucine	220014	268314	91526	575355	3036
Adenosine	27481	69440	17260	1404649	925160
Guanosine	2484	2593	3807	322899	144894
Phenprobamate	679550	1005854	775874	1257039	10856
Tuberostemonine	300892	555456	525932	455063	283580
L-tryptophan	92671	161310	133079	163463	40834
Salidroide	41459	67702	64416	53856	32779
Salidroside + NH_3	88351	145468	137597	111607	75283
Methyl 4-hydroxybenzoate	9170	27237	28549	30591	20074
p-coumaric acid	374263	537298	518972	407214	263705
Vanillic acid	81285	168227	181606	137018	68543
Norcantharidin	81284	168291	181596	137011	68512
Higenamine	83516	105990	107368	91255	58503
6-methylcoumarin	313149	455988	477787	421839	264078
Caffeic acid	209862	315156	316971	269357	183122
Ferulic acid	259704	375697	400387	312247	104415
Benzoylmesaconine	74271918	111058354	115423724	65234980	62682149
Benzoylhypacoitine	11173798	20504076	25449749	20971006	16650982
Neoandrographolide + HCOOH	143464	259580	224233	188300	73635
Mesaconitine	19635989	25672293	16326032	8592867	3459599
Hypaconitine	34141086	42983172	46925126	34294964	22862038
Aconitine	4638692	6134692	4606976	2414212	1031370

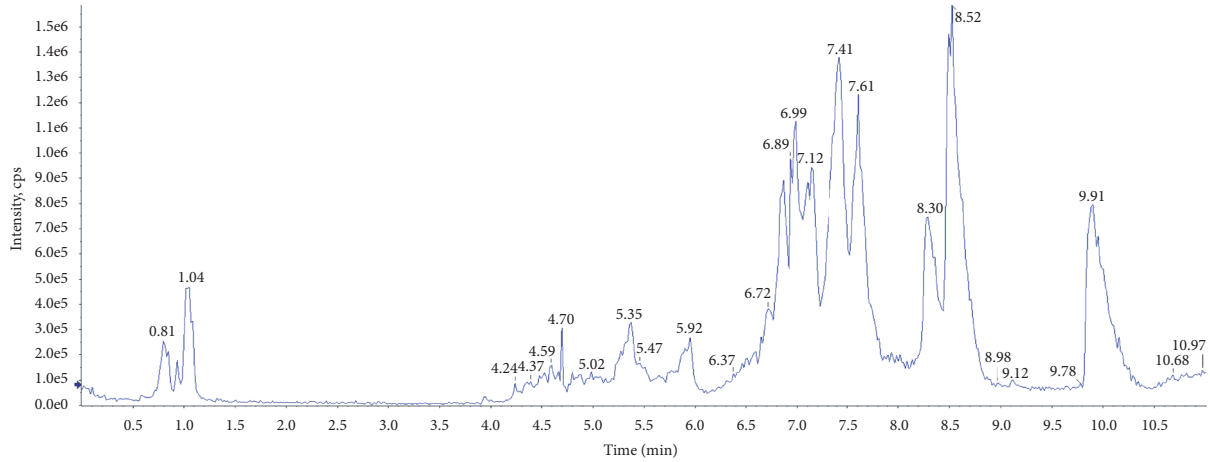

Figure 2: The TIC chromatograms of serum samples.

were extracted for alignment and normalization. Then, multivariate statistical analysis was carried out. LPS-DA was applied to model the four groups. As shown in Figure 3, the control group was well separated from groups A and B, suggesting that metabolic perturbation occurred significantly in the Fuzi group. Group C was closer to the control group, suggesting that glycyrrhizae could reduce the Fuzi-induced metabolic perturbation. As shown in Figure 4, the

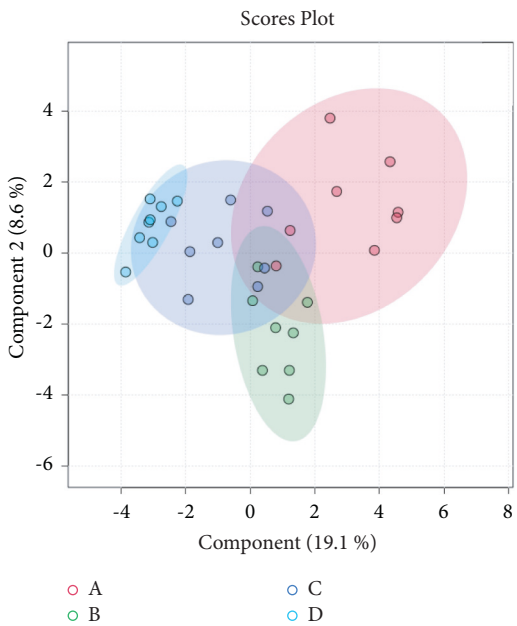

Figure 3: The partial least-squares discriminant analysis recognition method is based on serum metabolomic profiling.

heatmap based on the intensity levels of the metabolites among the four groups was used to clearly characterize the serum metabolites' profile. All differentiated metabolites ($p < 0.05$) in one-way ANOVA were selected. The one-way ANOVA plot is shown in Figure 5. The differential metabolites were hexadecanol, 2-hydroxyphenylacetate, 4-hydroxyphenyl acetate, 16-hydroxypalmitate, docosanoic acid, hexadecanal, hexadecanoic acid, hexadecenoic acid, icosapentaenoic acid, citrate, linoleate, N-acetyl-L-citrulline, N-acetyl-L-leucine, octadecatrienoic acid, octadecenoic acid, oleamide, phytanate, fluorocyclohexadiene, glycochenodeoxycholate-7-sulfate, suberic acid, taurochenodeoxycholate, and tetradecanoic acid. Pathway analysis was used to explore the metabolic pathway related to Fuzi toxicity. Linoleic acid metabolism, biosynthesis of unsaturated fatty acids, fatty acid biosynthesis, and the citrate cycle were disordered after the oral gavage of Fuzi (Figure 6).

4. Discussion

A simple, efficient, and sensitive method was established to identify the components of Fuzi decoction at different decocting times using the X500R QTOF system. A total of 35 compounds were found, including 3 diester alkaloids, 2 monoester alkaloids, 3 other alkaloids, 3 base compounds, 6 amino acids, 4 phenolic acids, 3 organic acids, 3 glycosides, and 3 sugars. There were also 5 other categories examined (1 vitamin, 1 coumarin, 1 lactone, 1 ester, and 1 anhydride). The results showed that the diester alkaloids in Fuzi gradually increased and reached the peak in 1~2 h and then decreased significantly. The monoester alkaloids also gradually increased and reached the peak at 2 h and then decreased significantly. Diester alkaloids with high toxicity are thermally unstable. They can be transformed into monoester alkaloids and further transformed into other alkaloids. This suggests that Fuzi can effectively reduce toxicity after a decocting time of more than 2 h, thus providing useful information for the clinical use of Fuzi.

When used in clinical settings, Fuzi could cause cardiotoxins, neurotoxins, nausea, palpitations, dizziness, vomiting, arrhythmia, hypotension, asystole, shock, coma, and neuron apoptosis among others [19, 20]. Aconitine, mesaconitine, and hypaconitine are the pharmacological and toxic components in Fuzi [21, 22]. In order to explore the effect of Fuzi on serum metabolites, the Fuzi decoction at 2 h was used for the metabolomics study. In clinical settings, glycyrrhizae could alleviate the side effects of Fuzi. In this study, it was used to validate the potential biomarker related to the toxicity of Fuzi.

In our study, pseudotargeted metabolomics was used to investigate the effect of glycyrrhizae on Fuzi-induced toxicity. The pseudotargeted method combines nontargeted and targeted analysis, which has proven to be a high-quality and information-rich method [23]. From analyzing the metabolomics study, the levels of 22 differential serum metabolites became abnormal (as seen in the Supplementary Materials section (available here), where there is a box plot chart of 22 metabolites), and the metabolite profiles of 22 candidate biomarkers were obtained from the quantitative analysis of the subjects. The figure was obtained using GraphPad Prism, and the names of the metabolites are shown in the box plot. The box plot consists of the median (i.e., horizontal line) and the interquartile range, and the whiskers indicate the minimum and maximum values unless there are outliers, in which case the whiskers extend to a maximum of 1.5 times the interquartile range. The 17 serum metabolites, including tetradecanoic acid, taurochenodeoxycholate, suberic acid, phytanate, octadecatrienoic acid, N-acetyl-L-leucine, N-acetyl-L-citrulline, linoleate, icosapentaenoic acid, hexadecenoic acid, hexadecenoic acid, glycochenodeoxycholate-7-sulfate, docosanoic acid, isocitrate, 16-hydroxypalmitate, 4-hydroxyphenyl acetate, and 2-hydroxyphenylacetate, were upregulated in groups A and B. Their contents were significantly higher than that of group D. However, their content in group C was closer to that of group D. This indicated that they were all close to the normal level after glycyrrhizae intervention. The 5 serum metabolites, including oleamide, octadecenoic acid, hexadecanal, fluorocyclohexadiene, and 1-hexadecanol, were downregulated in groups A and B. Their contents were significantly lower than that of group D. However, the content in group C was closer to that of group D. It also indicated that they were all close to the normal level after glycyrrhizae intervention. Therefore, the 22 differential metabolites were related to Fuzi. When Fuzi treatment was combined with the administration of glycyrrhizae, the concentrations of the 22 differential metabolites returned close to their normal levels. In previous studies, glycyrrhizae could delay the absorption of Fuzi or accelerate the metabolism of aconitine, mesaconitine, and hypaconitine to reduce the toxicity of Fuzi [24–28]. Other mechanisms may also be involved [29]. Sun et al. investigated the effect of glycyrrhizae in the attenuation

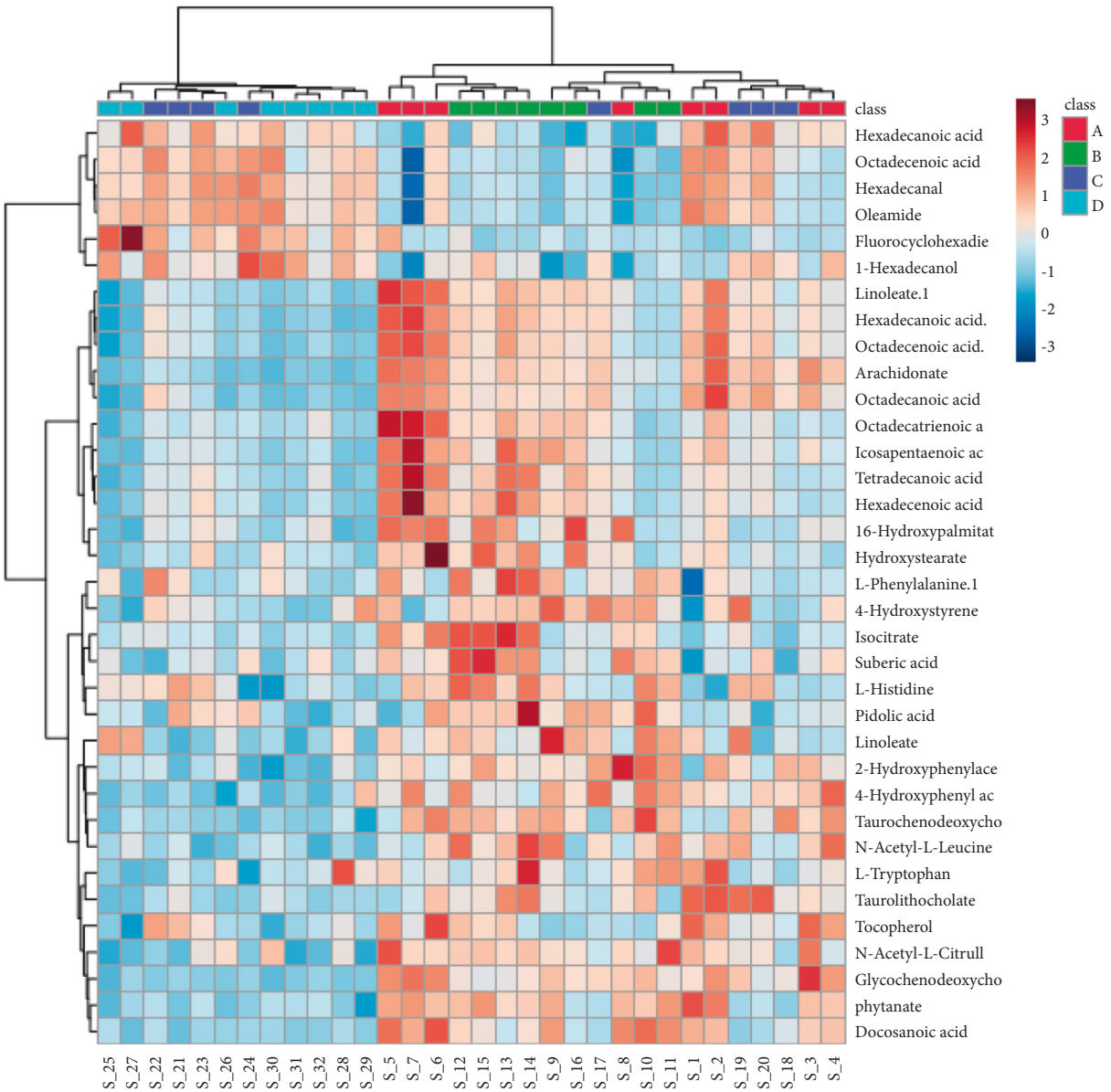

Figure 4: The hierarchical clustering heatmap of the potential biomarkers.

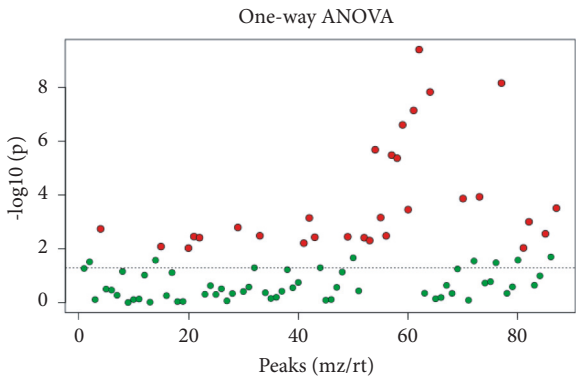

Figure 5: One-way ANOVA of the four groups.

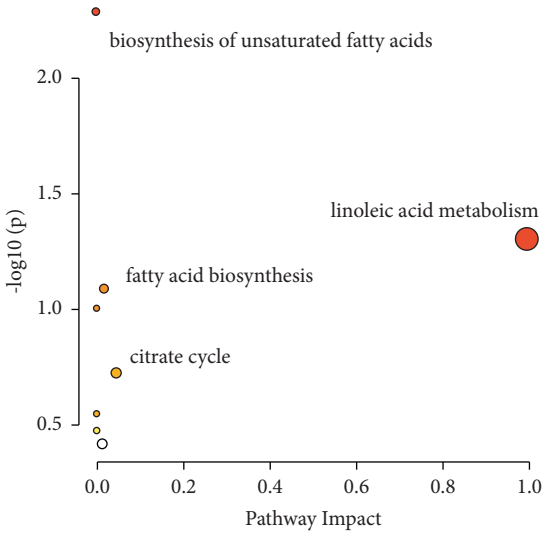

Figure 6: The metabolic pathways related to Fuzi poisoning.

of toxicity in rats induced by Fuzi using the NMR-based metabonomics method [30]. In our study, after pathway analysis, many metabolic pathways, including linoleic acid metabolism, biosynthesis of unsaturated fatty acids, fatty acid biosynthesis, and citrate cycle, were seriously impacted by Fuzi. Glycyrrhizae could regulate the disrupted citrate cycle (i.e., the central metabolic energy pathway) and fatty acid metabolism.

5. Conclusions

In our study, a total of 35 components in Fuzi were identified using UPLC-QTOF. Pseudotargeted metabolomics was used to detect the effects of glycyrrhizae on Fuzi-induced toxicity in rats. The results showed that amino acids and organic acids were significantly altered by Fuzi administration in rats. Glycyrrhizae could mitigate these metabolic changes, indicating that glycyrrhizae administration could reduce the toxicity of Fuzi at the metabolic level. The toxicity of Fuzi could be reduced at more than 2 h of decoction time. Our results demonstrate that glycyrrhizae reduces toxicity at the metabolic level through a series of pathways, such as linoleic acid metabolism, biosynthesis of unsaturated fatty acids, fatty acid biosynthesis, and citrate cycle.

Data Availability

The datasets generated during the present study are available from the corresponding author on reasonable request.

Ethical Approval

All experiments were performed in accordance with institutional guidelines and approved by the Health Authorities and Ethics Committees of the Hospital of Traditional Chinese Medicine of Zhongshan.

Consent

All subjects signed the informed consent prior to being included in the study.

Conflicts of Interest

The authors declare that they have no conflicts of interest regarding this publication.

Acknowledgments

This work was supported by the Science and Technology Development Project of Zhongshan (2020B1106).

Supplementary Materials

"Supplementary materials_MRMs" file includes the MRM transitions of 166 metabolites, such as their parent ions (Q1) and product ions (Q3). "Supplementary materials_the 22 metabolites" file includes the levels of 22 differential serum metabolites from the quantitative analysis of the subjects. (*Supplementary Materials*)

References

[1] D. Normile, "Asian medicine, the new face of traditional Chinese medicine," *Science*, vol. 299, pp. 188–190, 2003.

[2] R. Stone, "Biochemistry. Lifting the veil on traditional Chinese medicine," *Science*, vol. 319, pp. 709-710, 2008.

[3] X. Liang, X. Chen, Q. Liang et al., "Metabonomic study of Chinese medicine Shuanglong formula as an effective treatment for myocardial infarction in rats," *Journal of Proteome Research*, vol. 10, no. 2, pp. 790–799, 2011.

[4] R. Kawasaki, W. Motoya, T. Atsumi, C. Mouri, N. Kakiuchi, and M. Mikage, "The relationship between growth of the aerial part and alkaloid content variation in cultivated *Aconitum carmichaelii* debeaux," *Journal of Natural Medicines*, vol. 65, no. 1, pp. 111–115, 2011.

[5] J. Singhuber, M. Zhu, S. Prinz, and B. Kopp, "Aconitum in traditional Chinese medicine: a valuable drug or an unpredictable risk?" *Journal of Ethnopharmacology*, vol. 126, no. 1, pp. 18–30, 2009.

[6] P. Chen, Y. Chen, J. Chen, H. Tong, and Z. Xu, "Exploration of toxicity reducing mechanism of aconite alkaloids during decoction process using liquid chromatography-mass spectrometry," *Chinese Journal of Chromatography*, vol. 31, no. 11, pp. 1087–1092, 2013.

[7] H. Luo, Z. Huang, X. Tang et al., "Dynamic variation patterns of aconitum alkaloids in daughter root of *Aconitum carmichaelii* (fuzi) in the decoction process based on the content changes of nine aconitum alkaloids by HPLC-MS-MS," *Iranian Journal of Pharmaceutical Research*, vol. 15, no. 1, pp. 263–273, 2016.

[8] Zh. Sui, Q. Li, L. Zhu et al., "An integrative investigation of the toxicity of *Aconiti Kusnezoffii* radix and the attenuation effect of its processed drug using a UHPLC-Q-TOF based rat serum and urine metabolomics strategy," *Journal of Pharmaceutical and Biomedical Analysis*, vol. 145, pp. 240–247, 2017.

[9] D. Zhao, Y. Shi, X. Zhu et al., "Identification of potential biomarkers from *Aconitum carmichaelii*, a traditional Chinese medicine, using a metabolomic approach," *Planta Medica*, vol. 84, no. 6/7, pp. 434–441, 2018.

[10] X. Wang, H. Wang, A. Zhang et al., "Metabolomics study on the toxicity of aconite root and its processed products using ultraperformance liquid-chromatography/electrospray-ionization synapt high-definition mass spectrometry coupled with pattern recognition approach and ingenuity pathways analysis," *Journal of Proteome Research*, vol. 11, no. 2, pp. 1284–1301, 2012.

[11] A. Zhang, H. Sun, Z. Wang, W. Sun, P. Wang, and X. Wang, "Metabolomics: towards understanding traditional Chinese medicine," *Planta Medica*, vol. 76, no. 17, pp. 2026–2035, 2010.

[12] X. Wang, H. Sun, A. Zhang, W. Sun, P. Wang, and Z. Wang, "Potential role of metabolomics approaches in the area of traditional Chinese medicine: as pillars of the bridge between Chinese and Western medicine," *Journal of Pharmaceutical and Biomedical Analysis*, vol. 55, no. 5, pp. 859–868, 2011.

[13] K. Suhre, S. Y. Shin, A. K. Petersen et al., "Human metabolic individuality in biomedical and pharmaceutical research," *Nature*, vol. 477, no. 7362, pp. 54–60, 2011.

[14] R. Amathieu, P. Nahon, M. Triba et al., "Metabolomic approach by 1H NMR spectroscopy of serum for the assessment of chronic liver failure in patients with cirrhosis," *Journal of Proteome Research*, vol. 10, no. 7, pp. 3239–3245, 2011.

[15] H. Shen, J. Wu, L. Q. Di et al., "Enhancement by glycyrrhizae radix of hepatic metabolism of hypaconitine, a major

bioactive and toxic component of aconiti laterlis radix, evaluated by HPLC-TQ-MS/MS analysis," *Biomedical Chromatography*, vol. 27, no. 5, pp. 556–562, 2013.

[16] Y. Zhang, X. Bian, J. Yang, H. Wu, J. L. Wu, and N. Li, "Metabolomics of clinical poisoning by aconitum alkaloids using derivatization LC-MS," *Frontiers in Pharmacology*, vol. 10, p. 275, 2019.

[17] J. Song, X. Wang, Y. Guo et al., "Novel high-coverage targeted metabolomics method (SWATHtoMRM) for exploring follicular fluid metabolome alterations in women with recurrent spontaneous abortion undergoing in vitro fertilization," *Scientific Reports*, vol. 9, no. 1, p. 10873, 2019.

[18] Q. H. Xuan, C. Hu, D. Yu et al., "Development of A High coverage pseudotargeted lipidomics method based on ultra-high performance liquid chromatography-mass spectrometry," *Analytical Chemistry*, vol. 90, no. 12, pp. 7608–7616, 2018.

[19] T. Y. Chan, "Aconitum alkaloid content and the high toxicity of aconite tincture," *Forensic Science International*, vol. 222, no. 1–3, pp. 1–3, 2012.

[20] Y. Zhao, Q. Bu, Y. Zhou et al., "Mechanism study of aconitum-induced neurotoxicity in PC12 cells: involvement of dopamine release and oxidative damage," *Neurotoxicology*, vol. 31, no. 6, pp. 752–757, 2010.

[21] Y. Bao, F. Yang, and X. Yang, "CE-electrochemiluminescence with ionic liquid for the facile separation and determination of diester-diterpenoid aconitum alkaloids in traditional Chinese herbal medicine," *Electrophoresis*, vol. 32, no. 12, pp. 1515–1521, 2011.

[22] W. Liu, Z. Pi, X. Wang, F. Song, and S. Liu, "HPLC/ESI-MSn and ESI-MS studies on the aconitum alkaloids in three Chinese medicinal herbs," *Journal of Separation Science*, vol. 33, no. 17-18, pp. 2898–2906, 2010.

[23] P. Luo, P. Yin, W. Zhang et al., "Optimization of large-scale pseudotargeted metabolomics method based on liquid chromatography-mass spectrometry," *Journal of Chromatography A*, vol. 1437, pp. 127–136, 2016.

[24] L. Chen, J. Yang, A. K. Davey, Y. X. Chen, J. P. Wang, and X. Q. Liu, "Effects of diammonium glycyrrhizinate on the pharmacokinetics of aconitine in rats and the potential mechanism," *Xenobiotica*, vol. 39, no. 12, pp. 955–963, 2009.

[25] M. Pei, X. Duan, and X. Pei, "Compatability chemistry of acid-alkaline pair medicine of Fuzi and Gancao in sini decoction," *China Journal of Chinese Materia Medica*, vol. 34, no. 16, pp. 2047–2050, 2009.

[26] H. Shen, L. Zhu, N. Yao, and J. Wu, "The effect of the compatibility of radix aconiti laterlis and radix glycyrrhizae on pharmacokinatic of aconitine, mesaconitine and hypacmitine in rat plasma," *Journal of Chinese Medicinal Materials*, vol. 34, no. 6, pp. 937–942, 2011.

[27] J. M. Zhang, W. Liao, Y. He, Y. He, D. Yan, and C. M. Fu, "Study on intestinal absorption and pharmacokinetic characterization of diester diterpenoid alkaloids in precipitation derived from Fuzi-gancao herb-pair decoction for its potential interaction mechanism investigation," *Journal of Ethnopharmacology*, vol. 147, no. 1, pp. 128–135, 2013.

[28] L. Y. Zhu, H. Shen, and J. Wu, "Effects of radix glycyrrhizae on in vitro liver metabolism of aconitine evaluated by LC-MS/MS," *Chinese Journal of Pharmaceutical Analysis*, vol. 32, pp. 19923–11928, 2012.

[29] C. Y. Ung, H. Li, Z. W. Cao, Y. X. Li, and Y. Z. Chen, "Are herb-pairs of traditional Chinese medicine distinguishable from others? Pattern analysis and artificial intelligence classification study of traditionally defined herbal properties," *Journal of Ethnopharmacology*, vol. 111, no. 2, pp. 371–377, 2007.

[30] B. Sun, X. Wang, R. Cao et al., "NMR-based metabonomics study on the effect of gancao in the attenuation of toxicity in rats induced by Fuzi," *Journal of Ethnopharmacology*, vol. 193, pp. 617–626, 2016.

Hindawi
Evidence-Based Complementary and Alternative Medicine
Volume 2022, Article ID 5731372, 12 pages
https://doi.org/10.1155/2022/5731372

Research Article

Gallic Acid Inhibits Mesaconitine-Activated TRPV1-Channel-Induced Cardiotoxicity

Shu Han,[1] Liyuan Bao,[1] Weifei Li,[2] Kaiyang Liu,[1] Ya'nan Tang,[1] Xitao Han,[1] Ziqin Liu,[1] Hongyue Wang,[1] Fengting Zhang,[1] Shuo Mi,[1] and Hong Du[1]

[1]*School of Chinese Materia Medica, Beijing University of Chinese Medicine, Beijing 102488, China*
[2]*China Beijing Tong Ren Tang (Group) Co., Ltd., Beijing 100062, China*

Correspondence should be addressed to Hong Du; duhong@vip.163.com

Received 29 November 2021; Accepted 29 March 2022; Published 13 April 2022

Academic Editor: Francesca Menichetti

Aconiti Kusnezoffii Radix (Caowu) is often combined or processed with *Chebulae Fructus* (Hezi) to achieve attenuation purposes in Mongolian medicine. Mesaconitine (MA), a main bioactive ingredient of Caowu, is also famous for its high cardiotoxicity while exerting good anti-inflammatory and analgesic properties. Gallic acid (GA), one of the leading chemical components in Hezi, possesses cardiac protection. This study aimed to clarify the detoxification effects of GA from Hezi on MA-induced cardiotoxicity and whether the detoxification mechanism is related to the TRPV1 channel. Cell viability was determined by methyl thiazol tetrazolium (MTT), and lactate dehydrogenase (LDH) leakage rate was determined by ELISA. Hoechst 33258, JC-1, DCFH-DA, and Fluo-3 AM staining were conducted to detect apoptosis, mitochondrial membrane potential, reactive oxygen species (ROS), and Ca^{2+} respectively; TRPV1 channel current was recorded by whole-cell patch-clamp technology to observe the effect of GA and MA alone or in combination on TRPV1 channel. The results showed that GA exhibited pronounced detoxification effects on MA-induced cardiotoxicity. GA significantly inhibited the MA-induced decrease in cell viability; suppressed the MA-induced LDH leakage rate, apoptosis, and the release of ROS and Ca^{2+}; and alleviated the reduction of mitochondrial membrane potential. We found that MA-induced cardiotoxicity was significantly attenuated in H9c2 cells pretreated with the TRPV1 antagonist BCTC. In the whole-cell patch-clamp experiment, the TRPV1 channel current increase was caused by the GA and MA treatment, whereas it was reduced by the cotreatment of GA and MA. Our data demonstrate that GA in Hezi can reduce MA-induced cardiotoxicity by inhibiting intracellular Ca^{2+} influx, restoring mitochondrial membrane potential, and reducing apoptosis. The detoxification mechanism may be related to the desensitization of the TRPV1 channel by the combined application of MA and GA.

1. Introduction

Aconiti *k*usnezoffii *Radix* (Caowu), the root of *Aconitum kusnezoffii* Reichb., has been widely used in clinical practice in traditional Chinese medicine (TCM) as well as in Mongolian and Tibetan medicine for treating rheumatoid arthritis, joint pain, rheumatic fever, cancer, and other symptoms for thousands of years [1–6]. Caowu has both medicinal value and high toxicity. Down the ages, various methods, including decoction, compatibility, and processing, were developed to ensure the ideal balance of safety and effectiveness [7, 8]. However, in the clinic, Caowu-induced poisoning still occurs from time to time because of the narrow therapeutic index [9–11].

In Mongolian medicine, Caowu is often combined or processed with Chebulae Fructus (Hezi) to achieve attenuation purposes [12, 13]. Hezi, the fruits of *Terminalia chebula* Retz. and *Terminalia chebula* Retz, var. *tomentella* Kurt, is an ethnodrug that has long been used in the Mongolian area of China. Local clinical evidence has indicated that Hezi has preventative effects on toxicity from Caowu [14]. Our previous research further supported this view because we have observed the acute toxicity of the raw Caowu and Hezi-processed Caowu on mice, also examined

the effects on the survival rate of H9c2 cells, and found that the toxicity of Hezi-processed Caowu is significantly lower than that of raw Caowu [15, 16]. However, just as the mechanism of Caowu poisoning is still ambiguous, until now, there is a lack of explanations on Hezi relieving the toxicity of Caowu.

The principal active ingredients in Caowu are alkaloids with a C_{19}-diterpenoid skeleton, including aconitine (AC), mesaconitine (MA), and hypaconitine (HA) [17]. MA is the most abundant and representative component of alkaloids in Caowu [6]. Despite the therapeutic benefits, MA is one of the well-known cardiotoxins, which can cause lethal arrhythmias [18–20].

Gallic acid (GA) is one of the main chemical components in Hezi [21]. GA possesses multiple pharmacological potentials, such as anti-inflammatory, anti-oxidant, anti-viral, cardiac protection, and so on [22, 23]. It has been proven that GA can alleviate arrhythmias induced by aconitine, but the specific detoxification mechanism needs to be further studied [24].

Transient receptor potential vanilloid-1 (TRPV1), a calcium ion channel activated by the botanical irritant capsaicin, endovanilloids, H^+, organic acids, and temperature 42°C [25–27], has been implicated as a potential mediator of cardiomyocytes apoptosis because the direct activation of TRPV1 channel on the cardiomyocytes increases $[Ca^{2+}]i$, enhances the superoxide production by mitochondria, and reduces the mitochondrial membrane potential [28–31]. Some studies have also suggested that TRPVs are potential molecular targets for treating *Aconitum* species poisoning [32–35]. However, whether the TRPV1 channel and the precise molecular mechanism mediate the protective effect of Hezi against Caowu poisoning remains to be elucidated.

Therefore, in this study, we evaluated the detoxification effects of GA from Hezi on MA-induced H9c2 cells injury, and the detoxification mechanism by regulating the TRPV1 channel was explored in detail. We investigated the changes in H9c2 cells viability by methyl thiazol tetrazolium bromide (MTT) assay and measured the lactate dehydrogenase (LDH) leakage. ELISA was used to elucidate further the mediation of nuclear, intracellular calcium ions, intracellular ROS, and mitochondrial membrane potential. Besides, TRPV1 current was recorded by whole-cell patch-clamp technology, as a direct observe the effect of GA and MA alone or in combination on the TRPV1 channel.

2. Materials and Methods

2.1. Materials. Mesaconitine (molecular formula: $C_{33}H_{45}NO_{11}$; purity >99.8%) and gallic acid (molecular formula: $C_7H_6O_5$; purity >99.8%) were obtained from Chengdu DeSiTe Biotechnology Co. Ltd. (Sichuan, China). BCTC (molecular formula: $C_{20}H_{25}ClN_4O$; purity ≥98%) was purchased from AbMole (AbMole, Houston, United States). All the compounds above were dissolved in dimethyl sulfoxide (DMSO, Sigma, USA) as a stock solution, sonicated for 10 min, and then diluted in Dulbecco's modified eagle's medium (DMEM; Lablead, Beijing, China) to the corresponding concentration when used. The final concentration of DMSO was lower than 0.1% (v/v).

2.2. Cell Cultures and Experimental Grouping. H9c2 cells (Cell Resource Center, IBMS, CAMS/PUMC, Beijing, China) were cultivated in DMEM supplemented with 10% fetal bovine serum (FBS) and 1% (v/v) penicillin/streptomycin solution in a humidified incubator at 37°C in a 5% carbon dioxide (CO_2) atmosphere. When growing to the logarithmic phase, cells are either passaged or seeded (80~90% cell density).

Experimental grouping: (1) control group: H9c2 cells were cultured for 24 h without any treatment; (2) MA group: H9c2 cells were treated with 250 μM MA for 24 h; (3) BCTC + MA group: H9c2 cells were pretreated with BCTC (10 μM) for 30 min before 250 μM MA; and (4) GA + MA group: H9c2 cells were treated with 250 μM MA and different concentrations of GA (25, 50, and 100 μM) for 24 h.

2.3. Cell Viability and LDH Leakage Rate Assays. Cell viability and LDH leakage rate were determined by MTT assay (Beyotime Institute of Biotechnology, Shanghai, China) and measured the LDH release (Beyotime Institute of Biotechnology, Shanghai, China), respectively. Briefly, H9c2 cells were seeded at a density of 1×10^4 cells per well in 96-well plates and incubated in an incubator at 37°C with 5% CO_2 for 24 h. After treatment as described in Section 2.2, 100 μL MTT (0.5 mg/mL) solution was added, before incubation for 4 h in darkness; then 150 μL DMSO was used to lyse MTT formazan. Each well's optical density (OD) was measured at 490 nm using a microplate reader (BMG Labtech, Offenburg, Germany). LDH leakage rate from cell supernatants was measured using the LDH cytotoxicity kit according to the manufacturer's instructions. The optical density of each well was measured with a microplate reader (BMG Labtech, Offenburg, Germany) at a wavelength of 490 nm, and the LDH leakage rate (%) was calculated.

2.4. Apoptosis Morphology Assay. Hoechst 33258 kit (Beyotime Institute of Biotechnology, Shanghai, China) was used to determine the morphological changes of apoptosis. Briefly, H9c2 cells were seeded in 24 well plates at a density of 5×10^4 cells/well and incubated for 24 h. According to the manufacturer's instruction after treatment as described in Section 2.2, the images of nuclear morphological changes in the cells were taken under the Olympus fluorescence microscope (magnification, ×100, Nikon, Japan) at a 461 nm emission. The data were analyzed to represent the mean fluorescence intensity (MFI) with ImageJ software.

2.5. Intracellular ROS Assessment. Detection of intracellular ROS was performed using a dichloro-dihydro-fluorescein diacetate (DCFH-DA) kit (Beyotime Institute of Biotechnology, Shanghai, China). In brief, after H9c2 cells were treated as described in Section 2.2, the medium was removed, added 10 μM DCFH-DA, and incubated for 30 min at 37°C. Subsequently, the cells were washed with a serum-

free medium, and the images were taken under the fluorescence microscope (magnification, ×100, Nikon, Japan). The data were analyzed to represent the MFI with ImageJ software.

2.6. Mitochondrial Membrane Potential Measurement. The mitochondrial membrane potential changes in H9c2 cells were determined by JC-1 kit (Beyotime Institute of Biotechnology, Shanghai, China). In short, H9c2 cells were treated as described in Section 2.2, the H9c2 cells were incubated with JC-1 staining solution (10 μg/mL) for 20 min at 37°C in the dark and rinsed twice with PBS, and the images were taken under the fluorescence microscope (magnification, ×100, Nikon, Japan). The change of mitochondrial membrane potential was reflected by the ratio of red fluorescence to green fluorescence.

2.7. Intracellular Ca^{2+} Production Measurement. Changes in intracellular Ca^{2+} release were detected using the Fluo-3 AM kit (Beyotime Institute of Biotechnology, Shanghai, China). After treatment as described in Section 2.2, the H9c2 cells were incubated, loaded with a medium containing 5 μM Fluo-3AM (500 μL/well) for 60 min at 37°C in the dark, and rinsed with PBS; the images were taken under the fluorescence microscope (magnification, ×100, Nikon, Japan). The data were analyzed to represent the MFI with ImageJ software. Mean fluorescence intensity was used to evaluate the extent of Ca^{2+} efflux.

2.8. Whole-Cell Patch-Clamp Recording. TRPV1-HEK293 cells were cultured in DMEM medium supplemented with 10% FBS, 100 μg/mL Zeocin and 10 μg/mL Blastincidin in the culture dish. Cells grew in a humidified incubator at 37°C with 5% CO_2. For the manual patch-clamp test, the cells were detached using the TrypLE™ Express solution. Then 8×10^3 cells were seeded into a 24-well plate (final medium volume: 500 μL) with 1 coverslip in each well. The current was induced by tetracycline for 18 h. All cell culture procedures followed the cell culture SOP of ICE Bioscience Inc. TRPV1 receptor current was recorded at a holding potential of −70 mV with gap-free mode to record the peak current after the test article application from low to high concentrations. The brief experimental protocol is described as follows: the 10 μM Capsaicin and each concentration of GA and MA alone or in combination will be applied 1–2 times followed by a 1 min wash-in using the extracellular solution. The next test concentration will be tested.

The data will be collected by EPC-10 amplifier and stored in PatchMaster (HEKA) soft. Glass pipette was prepared with a micropipette puller. The glass pipette was manipulated using a micromanipulator under the microscope. After touching the cell, a slight suction was applied to achieve high seal resistance (GΩ). Fast capacitance (in pF) compensation was made after achieving a high seal, and the membrane was broken. After the whole-cell mode was achieved, cell capacitance (in pF) compensation was made from whole-cell capacitance compensation. No leak subtraction was made. The test and control solutions have flowed into a recording chamber mounted on the stage of an inverted microscope via a gravity-fed solution delivery system. Solution solutions were withdrawn from the recording chamber by vacuum aspiration during the experiment. Each concentration was tested multiple times. All the tests were performed at room temperature. The current value was standardized through the whole-cell capacitance and was shown using pA/pF.

2.9. Statistical Analysis. The experimental data were analyzed using GraphPad Prism software version 8.0.1 (GraphPad Software, Inc. La Jolla, USA) and ImageJ 1.8.0 (Bethesda, Maryland, USA). Statistically significant differences were performed through one-way analysis of variance (ANOVA), and Sidak test was used for pairwise comparison. The results were expressed as the mean ± standard deviation (SD). $P < 0.05$ was considered statistically significant.

3. Results

3.1. MA Inhibited Cell Viability in H9c2 Cells. As shown in Figure 1, 0–250 μM MA treatment for 24 h affected the proliferation of H9c2 cells to varying degrees. Compared with the control group, 25–250 μM MA reduced the survival rate of H9c2 cells in a concentration-dependent manner, especially at 250 μM, cell viability was significantly decreased to 61.88 ± 0.78%, indicating that MA could significantly inhibit the proliferation of H9c2 cells in the range of 25–250 μM. To further elucidate the toxic effect and mechanism of MA on H9c2 cells, 250 μM of MA was chosen in subsequent experiments.

3.2. GA Treatment Improved MA-Induced Cell Viability and Inhibited LDH Leakage Rate. Cell survival rate and LDH leakage rate were generally used as indicators of cytotoxicity [36]. To investigate the effect of GA on H9c2 cells toxicity induced by MA, the survival rate of H9c2 cells was measured. As shown in Figure 2(a), the results show that 250 μM MA significantly decreased the cell viability of H9c2 cells, and the survival rate was reduced to 61.85 ± 0.74% ($P < 0.01$). Treatment with GA at concentrations of 25, 50, and 100 μM significantly suppressed the decrease of cell viability in a concentration-dependent manner ($P < 0.01$), indicating that GA increased cell viability and protected cardiomyocytes against MA-induced injury. LDH is a stable enzyme expressed in the cytoplasm of myocardial cells [37]. When the cells are damaged, the cell membrane will be destroyed, and a large amount of LDH will be released. Therefore, the content of LDH in the cell supernatant can indirectly reflect the degree of cell damage. As shown in Figure 2(b), H9c2 cells could significantly promote the release of LDH in the cells after incubating with 250 μM MA. However, it can be blocked by 25, 50, and 100 μM GA, and the LDH leakage rate gradually decreases with the increase of concentration ($P < 0.01$).

To investigate the role of the TRPV1 channel in MA-induced H9c2 cells, we added BCTC, a TRPV1 channel

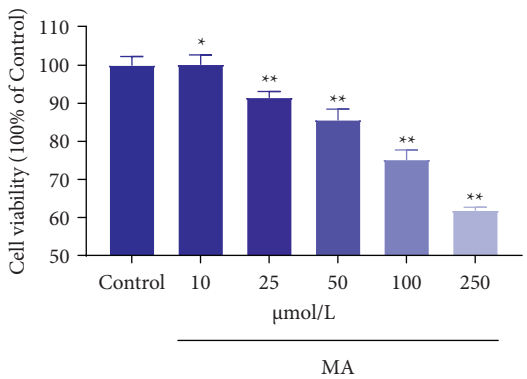

Figure 1: H9c2 cells were treated with various concentrations of MA for 24 h. Cell viability was quantified and expressed as a percentage of the control group. The viability of the control group was defined as 100%. Data are presented as the mean ± SD ($n = 3$). $^{*}P < 0.05$ versus control group and $^{**}P < 0.01$ versus control group.

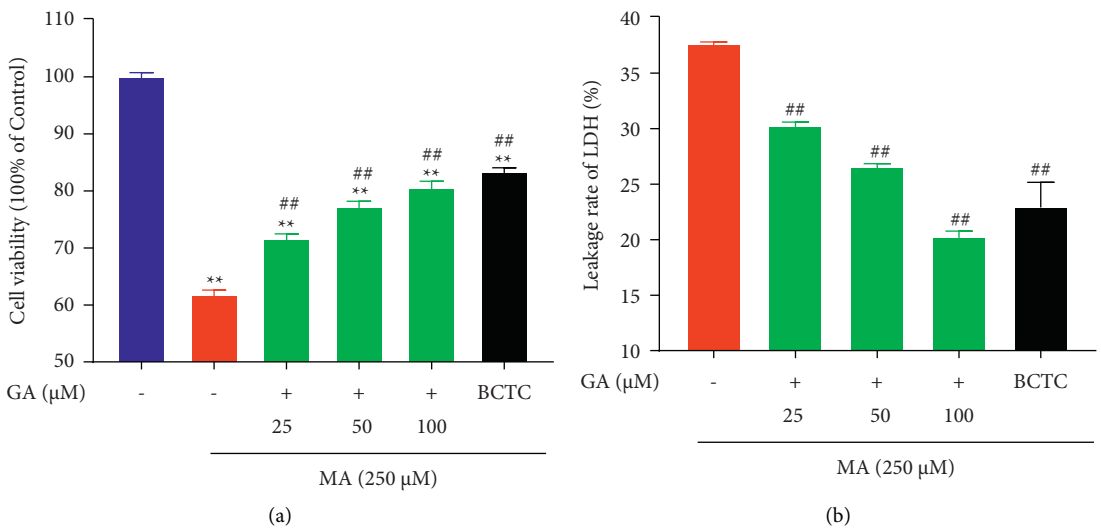

Figure 2: Effect of GA and the coadministrative of MA on the cell viability and LDH leakage rate. (a) Effects of GA (25, 50, and 100 μM) or pretreatment with BCTC (10 μM) on the decrease of cell viability in H9c2 cells induced by 250 μM MA. The viability of the control group was defined as 100%. (b) Effects of GA (25, 50, and 100 μM) or pretreatment with BCTC (10 μM) on the increase of LDH leakage rate in H9c2 cells induced by 250 μM MA. Data are presented as the mean ± SD ($n = 3$). $^{**}P < 0.01$ versus control group, and $^{\#\#}P < 0.01$ versus MA group.

antagonist [38]. Pretreatment with BCTC (i.e., TRPV1 channel blocking) significantly increased the viability of H9c2 cells and inhibited the leakage rate of LDH ($P < 0.01$). Our data showed that MA might exert some toxicity by mediating the TRPV1 channel.

3.3. GA Treatment Inhibited MA-Induced Apoptosis and ROS Release. The overproduction of ROS generally accompanies the occurrence of cardiotoxicity, and the accumulation of ROS can induce the generation of oxidative stress in cardiomyocytes and then induce the occurrence of apoptosis to a certain extent [39, 40]. To further explore the effect of GA on apoptosis and ROS in MA-induced H9c2 cells, we used DCFH-DA and Hoechst 33258 to detect the MA-induced ROS production and nuclear morphology changes in H9c2 cells, respectively. As shown in Figures 3(a) and 4, the nucleus of the control group showed uniform blue fluorescence. Many apoptotic cells appeared after being treated with 250 μM MA. The nucleus chromatin was pyknotic, showing bright blue fluorescence of dense concentration staining ($P < 0.01$). When the TRPV1 channel was blocked, the mean fluorescence intensity of the nucleus could be significantly reduced, and the damaged state of the nucleus could be improved ($P < 0.01$). After treatment with GA at a concentration of 25, 50, and 100 μM, it was found that the pyknosis of nuclear chromatin was significantly weakened, and the intensity of bright blue fluorescence of dense concentration staining gradually decreased with the increase of concentration ($P < 0.01$). As shown in Figures 3(b) and 5, compared with the control group, the green fluorescence of H9c2 cells treated with 250 μM MA was significantly increased; that is, the level of ROS in the cells increased ($P < 0.01$). When the TRPV1 channel was blocked, green fluorescence intensity was significantly attenuated, and ROS release was reduced ($P < 0.01$). After 24 h

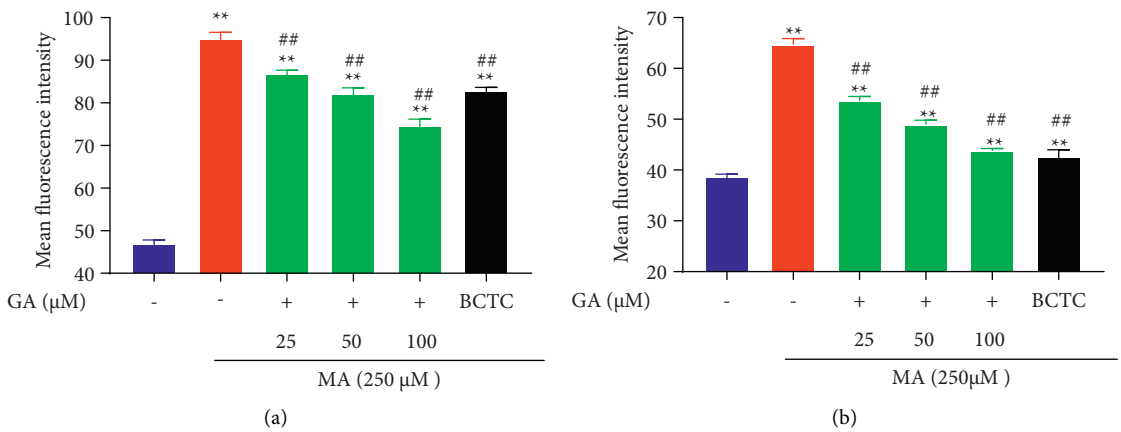

Figure 3: Effect of GA and the coadministrative of MA on the mean fluorescence intensity of nucleus and ROS in H9c2 cells. (a) Effects of GA (25, 50, and 100 μM) or pretreatment with BCTC (10 μM) on the increase of the mean fluorescence intensity of the nucleus in H9c2 cells induced by 250 μM MA. (b) Effects of GA (25, 50, and 100 μM) or pretreatment with BCTC (10 μM) on the increase of the mean fluorescence intensity of ROS in H9c2 cells induced by 250 μM MA. Data are presented as the mean ± SD ($n = 3$). $^{**}P < 0.01$ versus control group and $^{\#\#}P < 0.01$ versus MA group.

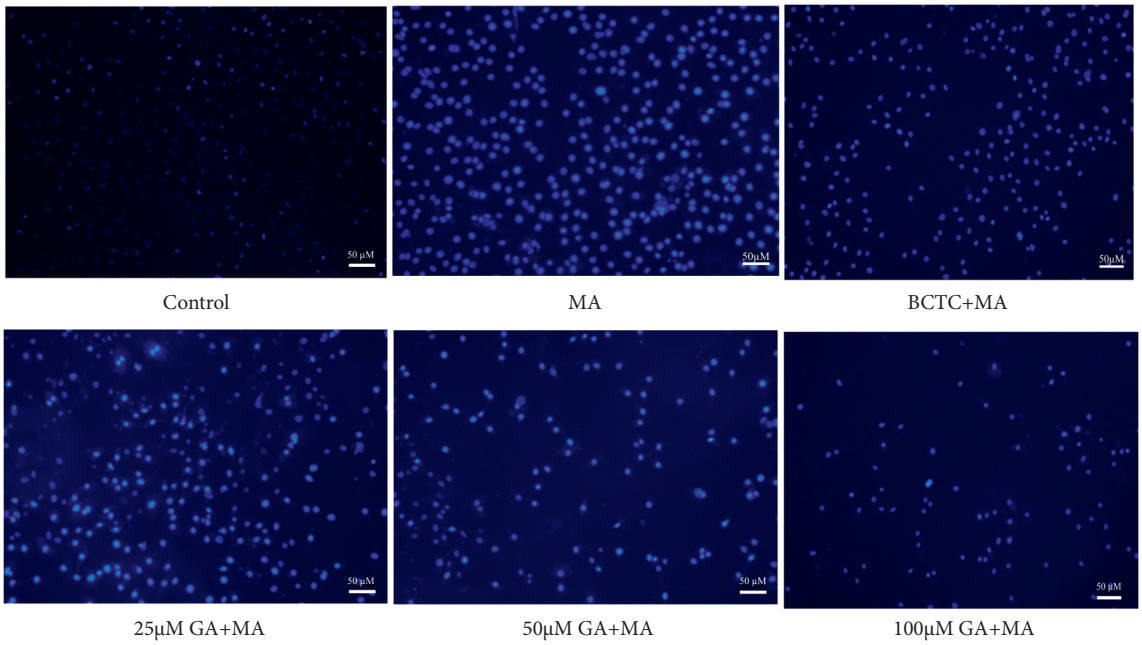

Figure 4: Effect of GA and the coadministrative of MA on the apoptosis in H9c2 cells. H9c2 cells were incubated with GA (25, 50, and 100 μM) or pretreated with BCTC (10 μM) in H9c2 cells induced by 250 μM MA. Nucleus fluorescence images are visualized by a fluorescence microscope (magnification, ×100; scale bar, 50 μm).

of treatment with GA (25, 50, and 100 μM), the green fluorescence intensity in the cells was lower than that of 250 μM MA in a concentration-dependent manner ($P < 0.01$).

3.4. GA Treatment Alleviated MA-Induced Mitochondrial Membrane Potential and Inhibited Ca^{2+} Release. Literature studies show that mitochondria are not only the central organ of cell metabolism and cell respiration, but also regulate the intracellular Ca^{2+} concentration. When the mitochondrial function is dysfunctional or damaged, it will lead to continuous Na^{+} influx in the cell, activate Na^{+}–Ca^{2+} exchange protein, increase the intracellular Ca^{2+} concentration, lead to intracellular calcium overload, and then lead to mitochondrial membrane depolarization, mitochondrial membrane potential reduction, and even cell death [41, 42]. Figures 6(a) and 7 show that the control group cells mostly showed red fluorescence and a small amount of green fluorescence, which indicated that the mitochondrial membrane potential was average. After treatment with 250 μM MA, the red fluorescence intensity decreased, and the green fluorescence intensity increased significantly, which significantly reduced the mitochondrial membrane

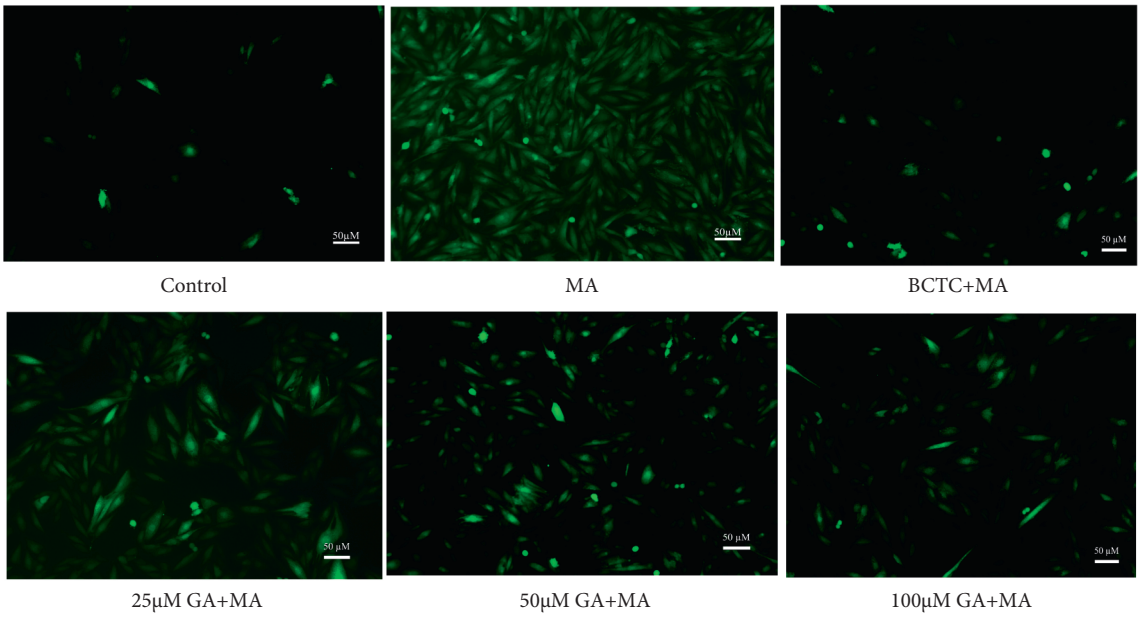

Figure 5: Effect of GA and the coadministrative of MA on the ROS in H9c2 cells. H9c2 cells were incubated with GA (25, 50, and 100 μM) or pretreated with BCTC (10 μM) in H9c2 cells induced by 250 μM MA. ROS fluorescence images are visualized by a fluorescence microscope (magnification, ×100; scale bar, 50 μm).

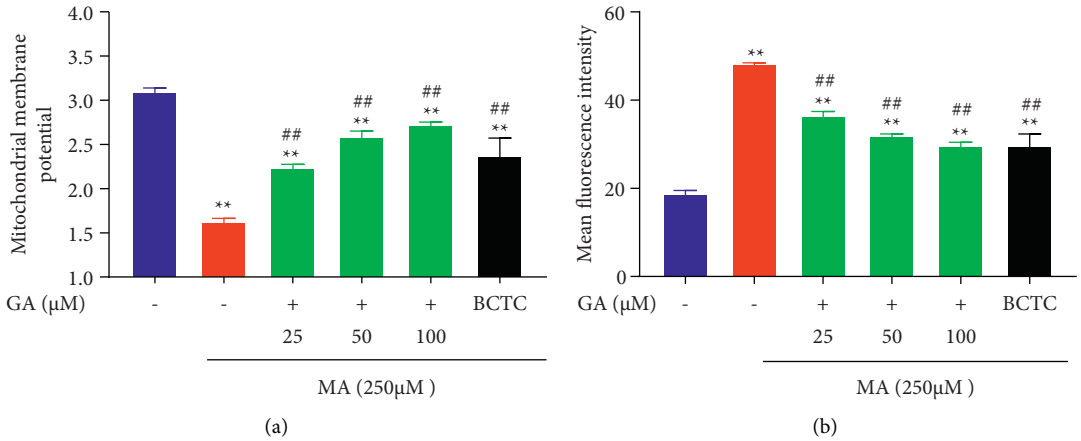

Figure 6: Effect of GA and the coadministrative of MA on the mitochondrial membrane potential and Ca^{2+} release in H9c2 cells. (a) Effects of GA (25, 50, and 100 μM) or pretreatment with BCTC (10 μM) on the decrease of the mitochondrial membrane potential in H9c2 cells induced by 250 μM MA. (b) Effects of GA (25, 50, and 100 μM) or pretreatment with BCTC (10 μM) on the increase of the mean fluorescence intensity of Ca^{2+} in H9c2 cells induced by 250 μM MA. Data are presented as the mean ± SD ($n = 3$). $^{**}P < 0.01$ versus control group and $^{\#\#}P < 0.01$ versus MA group.

potential ($P < 0.01$), and increased mitochondrial membrane potential after TRPV1 channel blockade ($P < 0.01$). After treatment with GA at a concentration of 25, 50, and 100 μM, the cells' red fluorescence/green fluorescence ratio was enhanced, and the mitochondrial membrane potential increased dose-dependent ($P < 0.01$). As shown in Figures 6(b) and 8, compared with the control group, the green fluorescence of H9c2 cells treated with 250 μM MA was significantly increased, that is, the intracellular Ca^{2+} release increased significantly ($P < 0.01$); inhibiting the sustained Ca^{2+} influx when TRPV1 channel was blocked ($P < 0.01$). After treatment with GA (25, 50, and 100 μM), the green fluorescence intensity in the cells decreased in a concentration-dependent manner ($P < 0.01$).

3.5. Effects of MA, GA, and the Combination of Both on TRPV1 Channel Current. To further explore the mechanism by which GA alleviates MA-induced cardiotoxicity, we also evaluated the effects of MA, GA, and the combination of both on TRPV1 channel current by a whole-cell patch clamp. As shown in Figures 9(a) and 9(b), the TRPV1 current could be activated by 10 μM capsaicin, an agonist of the TRPV1 channel. When the concentration of MA was

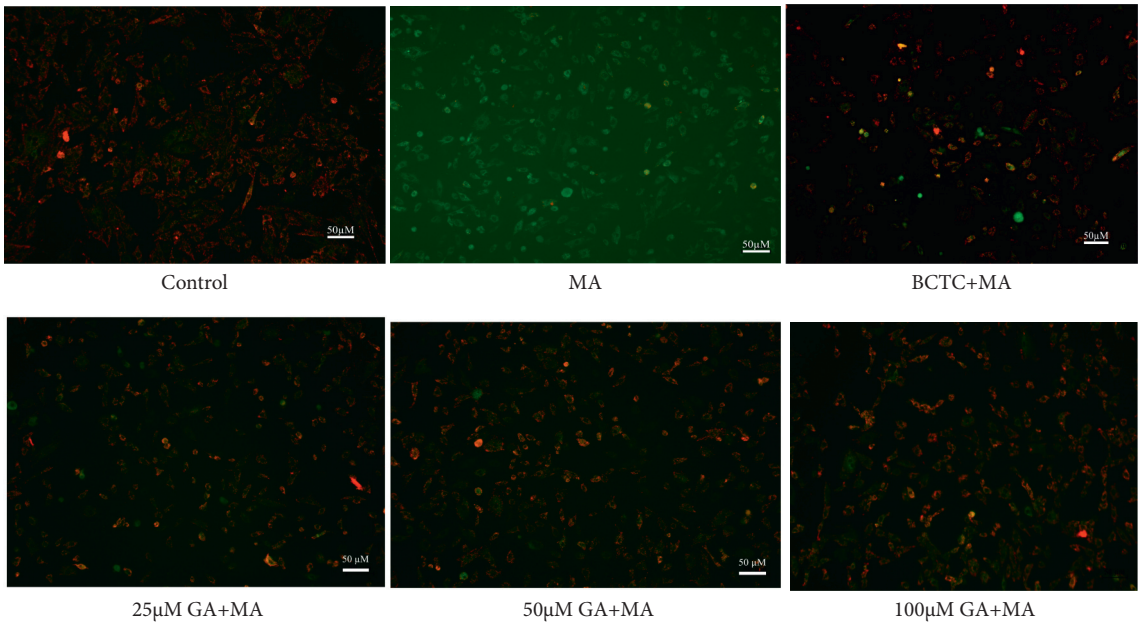

Figure 7: Effect of GA and the coadministrative of MA on the mitochondrial membrane potential of H9c2 cells. H9c2 cells were incubated with GA (25, 50, and 100 μM) or pretreated with BCTC (10 μM) in H9c2 cells induced by 250 μM MA. Mitochondrial membrane potential fluorescence images are visualized by a fluorescence microscope (magnification, ×100; scale bar, 50 μm).

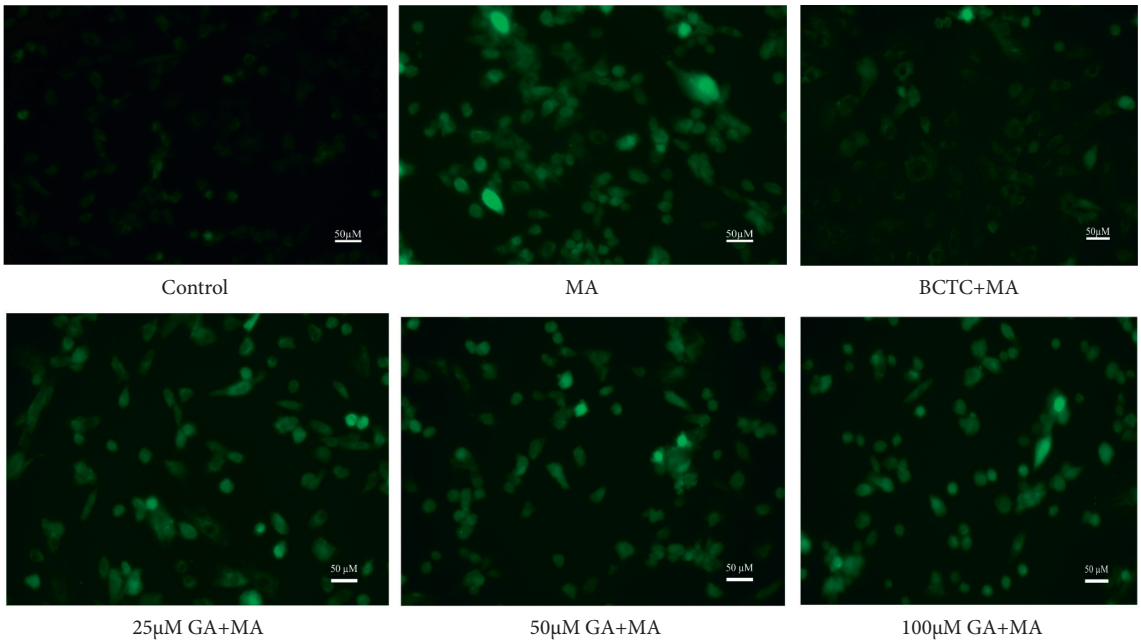

Figure 8: Effect of GA and the coadministrative of MA on the Ca^{2+} release in H9c2 cells. H9c2 cells were incubated with GA (25, 50, and 100 μM) or pretreated with BCTC (10 μM) in H9c2 cells induced by 250 μM MA. Ca^{2+} release fluorescence images are visualized by a fluorescence microscope (magnification, ×100; scale bar, 50 μm).

25 μM, a significant TRPV1 channel current was generated with a current density of −80.68 ± 6.51, which increased to −91.53 ± 6.77 as the concentration increased. TRPV1 channel current was elicited when GA was present at a concentration of 5 μM; with the increase of concentration, the current increased significantly, as shown in Figures 9(c) and 9(d). It suggests that similar to capsaicin, both MA and GA can act as agonists for the TRPV1 channel.

It can be seen from Figure 10 that when MA and GA are applied in combination, 50 μM MA can produce a prominent TRPV1 channel current. Compared with the MA Group, 5 μM GA reduced the intensity of TRPV1 current

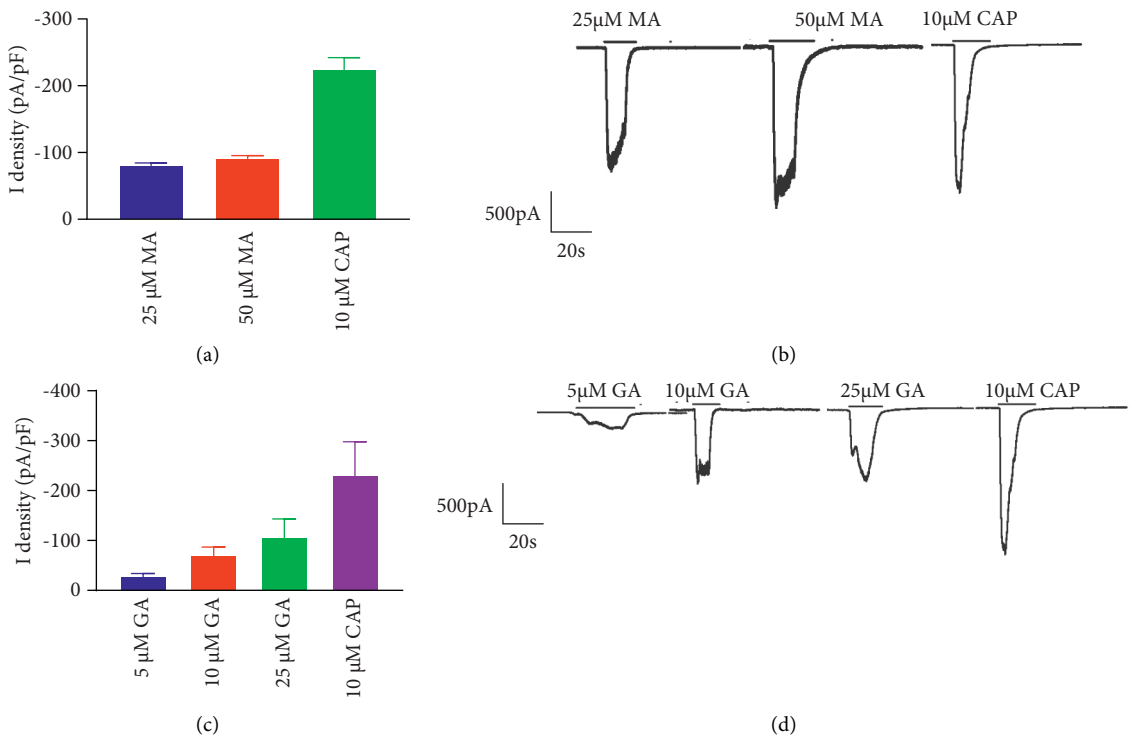

Figure 9: Current changes in TRPV1-HEK293 cells treated with MA and GA alone. (a) and (c) The bar graph shows the quantified data by calculating the current densities. (b) and (d) Representative traces of MA (25 and 50 μM) and GA (5, 10, and 25 μM) in TRPV1-HEK293 cells. The current densities are presented as the mean ± SD ($n = 3$). The holding potential used was −70 mV. CAP: capsaicin, MA: mesaconitine, and GA: gallic acid.

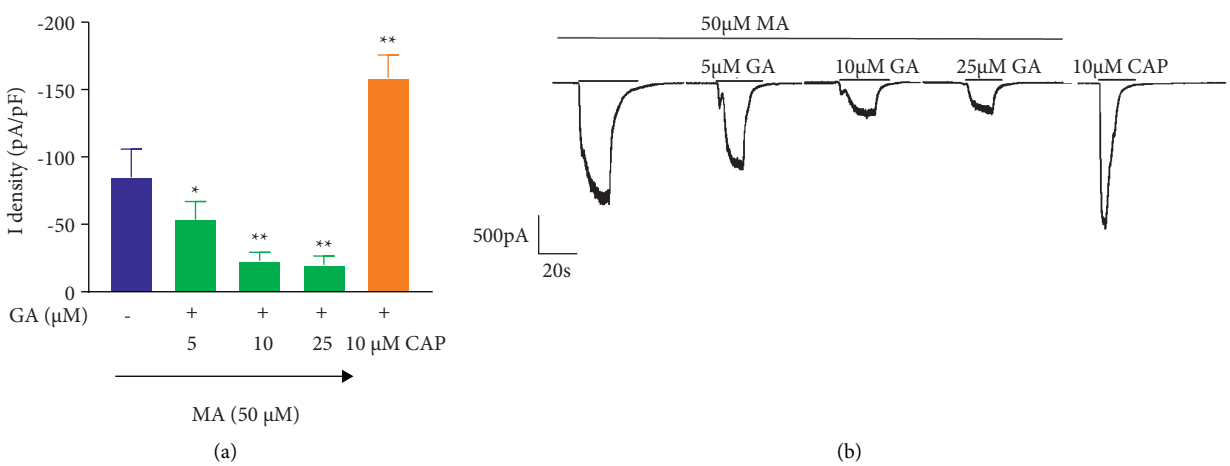

Figure 10: Changes of current in TRPV1-HEK293 cells cotreated with GA (5, 10, and 25 μM) and MA (50 μM). (a) The bar graph shows the quantified data by calculating the current densities. (b) GA (5, 10, and 25 μM) and the co-administrative of 50 μM MA on the representative traces in TRPV1-HEK293 cells. The current densities are presented as the mean ± SD ($n = 3$). $^{*}P < 0.05$ versus MA group and $^{**}P < 0.01$ versus MA group. The holding potential used was −70 mV.

($P < 0.05$) and further inhibited the intensity of TRPV1 current with the increase of concentration ($P < 0.01$).

4. Discussion

Mesaconitine, a main active ingredient of Caowu, is notorious for its high cardiotoxicity and neurotoxicity, of which cardiotoxicity is the primary toxic reaction, which could result in arrhythmia, ventricular tachycardia (VT), ventricular fibrillation (VF), and even sudden death if used excessively [43–47]. Previous studies have demonstrated the mechanisms by which MA induces cardiotoxicity are as follows: (1) blocking the inactivation of voltage-dependent sodium channels and prolonging potential action durations (APDs) and (2) acetylcholine released by exciting the vagus nerve will directly inhibit the atrioventricular node or excite

the ectopic pacemaker, thereby leading to arrhythmia [48–51].

The TRPV1 channel is a thermosensitive channel that can be activated by Aconitum plants and components such as capsaicin and aconitine, which in turn can induce apoptosis, Ca^{2+} overload, and so on, leading to a certain degree of toxicity [52–55]. Some literature also suggested that one of the causes of cardiotoxicity of Caowu may also be related to the activation of TRPV1 channel [31, 33, 34]. Meanwhile, our experiments also proved this notion: activation of TRPV1 channel induced by MA could accelerate the generation of apoptosis, decrease the mitochondrial membrane potential, and intracellular Ca^{2+} overload, which was significantly reversed by BCTC, a TRPV1 antagonist. All the above indicate that myocardial injury is significantly aggravated when TRPV1 channel is activated.

It was reported that the TRPV1 channel is subject to dose-dependent sensitization or desensitization, that is to say, low-dose agonists can sensitize the TRPV1 channel. On the other hand, the TRPV1 channel can be desensitized upon prolonged activation or repeated exposures to agonists [56, 57]. As a protective mechanism, desensitization of the TRPV1 channel can reduce the occurrence of cardiotoxicity by inhibiting a large amount of Ca^{2+} influx to some degree [58, 59], GA was found to reduce MA-induced cardiotoxicity by improving cell viability; inhibiting LDH, ROS, Ca^{2+}, as well as apoptosis; and alleviating the reduction of mitochondrial membrane potential in this study, whether the exertion of the detoxification effect is also related to the desensitization mechanism deserves to be explored. To further elucidate this, we measured the TRPV1 channel activity by measuring TRPV1 channel current upon GA and MA treatment, respectively, and cotreatment in TRPV1-HEK293 cells. In TRPV1-HEK293 cells, the TRPV1 channel current increase was caused by the GA and MA treatment, whereas it was reduced by the cotreatment of GA and MA. Furthermore, as shown in the above studies, when MA is combined with GA, it can reduce the cardiotoxicity induced by MA. so this study speculated that the mechanism of action of GA to attenuate MA-induced cardiotoxicity might be due to the synergistic effect of MA and GA to desensitize TRPV1 channel to exert an attenuated effect partially.

TRPV1 channel is also a target for pain treatment, and its analgesic effect is mainly achieved by inactivating the TRPV1 channel or chronic desensitization [60]. Clinical studies have shown that *Aconitum* herbs can inhibit anti-inflammatory and analgesic effects, also related to the TRPV1 channel [32]. Our experiment found that the combination of gallic acid and mesaconitine could achieve a particular desensitization effect on TRPV1 channels to reduce cardiotoxicity by inhibiting the influx of calcium ions in cardiomyocytes. However, whether the desensitization caused by the combination of gallic acid and mesaconitine also has a specific analgesic effect needs to be verified by further experiments.

This study also had some limitations. On the one hand, although we found that GA, the main active component in Hezi, can reduce the cardiotoxicity induced by MA, the leading active ingredient in Caowu, whether other chemical components in Caowu and Hezi can also play a similar role needs to be further confirmed. On the other hand, this study was conducted only at the cellular level and lacked whole animal experiments to corroborate. It should not be ignored that some works of literature have also proved that the occurrence of arrhythmias, tachycardias, and other phenomena induced by *Aconitum* species can also be partially reversed in the presence of a large number of calcium ions [61], which also provides a basis for our subsequent studies, that is, whether it will also reverse the arrhythmia effect induced by Caowu after processing or compatibility with Hezi in the clinical use is a question worthy of discussion. This will also provide a basis for the safe and rational use of *Aconitum* species in the clinic.

5. Conclusions

The aforementioned results show that the detoxification of MA-induced cardiotoxicity by GA can be achieved via increasing cell ability, suppressing the release of LDH, ROS, Ca^{2+}, and the occurrence of apoptosis, restoring mitochondrial membrane potential. In addition, this study also found that MA and GA could act as agonists for the TRPV1 channel similar to capsaicin, yet the TRPV1 channel current was reduced at the cotreatment of GA and MA. From this, we speculated that the detoxification of MA-induced cardiotoxicity by GA might be related to the desensitization of the TRPV1 channel by the combined application of MA and GA.

Abbreviations

MA:	Mesaconitine
GA:	Gallic acid
LDH:	Lactate dehydrogenase
MTT:	Methylthiazoltetrazolium bromide
ROS:	Reactive oxygen species
TRPV1:	Transient receptor potential vanilloid-1
TCM:	Traditional Chinese medicine
AC:	Aconitine
HA:	Hypaconitine
DMSO:	Dimethyl sulfoxide
DMEM:	Dulbecco's modified eagle's medium
FBS:	Fetal bovine serum
CO2:	Carbon dioxide
OD:	Optical density
MFI:	Mean fluorescence intensity
DCFH-DA:	Dichloro-dihydro-fluorescein diacetate
VT:	Ventricular tachycardia
VF:	Ventricular fibrillation
APDs:	Action potential durations.

Data Availability

The data used to support the findings of this study are available from the first author (hs361015@163.com) upon reasonable request.

Conflicts of Interest

All the authors declare that they have no competing interests.

Acknowledgments

This work was supported by grants from the National Natural Science Foundation of China (NSFC, 81774004) and the National Natural Science Foundation of China (NSFC, 82130113).

References

[1] National Pharmacopoeia Committee, *Pharmacopoeia of People's Republic of China (2020)*, China Medical Science and Technology Press, vol. 1, p. 247, Beijing, China, 2020.

[2] X. Zhao, Y.-R. Kim, Y. Min, Y. Zhao, K. Do, and Y.-O. Son, "Natural plant extracts and compounds for rheumatoid arthritis therapy," *Medicina*, vol. 57, no. 3, p. 266, 2021.

[3] A. P. Liu and Z. F. Yu, "Effects of Radix Aconiti Kusnezoffii on compound action potential of sciatic nerve of toad," *Lishizhen Medicine and Materia Medica Research*, vol. 19, no. 5, pp. 1109-1110, 2008.

[4] W. Wang, J. Li, and H. Liu, "A multi-center, randomized, controlled, non-inferiority clinical study of bulleyaconitine A in the treatment of mild and moderate cancer pain," *Chinese Journal of Preventive Medicine*, vol. 27, no. 3, pp. 188–195, 2021.

[5] S. S. Na, *Modern Mongolian Pharmacy*, Inner Mongolia University Press, vol. 1, p. 210, Huhhot, China, 2011.

[6] F. Liu, X. Tan, X. Han, X. Li, N. Li, and W. Kang, "Cytotoxicity of Aconitum alkaloid and its interaction with calf thymus DNA by multi-spectroscopic techniques," *Scientific Reports*, vol. 7, no. 1, p. 14509, 2017.

[7] S. Liu, W. F. Li, and Y. Li, "Specific analysis of Aconiti Kusnezoffii Radix processed with Fructus Chebulae with HPLC and quantification of its quality control ingredients," *Journal of Beijing University of Traditional Chinese Medicine*, vol. 40, no. 4, pp. 328–333, 2017.

[8] J. Wu, N. Lin, F. Li et al., "Induction of P-glycoprotein expression and activity by Aconitum alkaloids: implication for clinical drug-drug interactions," *Scientific Reports*, vol. 6, no. 1, p. 25343, 2016.

[9] S. Sheth, E. C. Tan, H. H. Tan, and L. Tay, "Herb-induced cardiotoxicity from accidental aconitine overdose," *Singapore Medical Journal*, vol. 56, no. 7, pp. e116–9, 2015.

[10] S. Han, L. Lv, and H. R. Wang, "Neurotoxicity of aconite in vivo and in vitro," *West China Journal of Pharmaceutical Sciences*, vol. 3, pp. 286–288, 2007.

[11] T. Chan, "Aconitum alkaloid poisoning related to the culinary uses of aconite roots," *Toxins*, vol. 6, no. 9, pp. 2605–2611, 2014.

[12] A. J. Zhao, H. Li, and Y. Tu, "Terminalia chebula combined with Aconitum kusnezoffii in different proportions compatibility to the content of three kinds of double ester type Aconitum alkaloids," *Journal of Changchun University of Chinese Medicine*, vol. 32, no. 4, pp. 697–700, 2018.

[13] Y. Lv, H. T. Zhang, and W. F. Guo, "Inheritance and development of traditional Mongolian medicine processing," *China Journal of Chinese Materia Medica*, vol. 44, no. 13, pp. 2742–2747, 2019.

[14] T. D. Ba, Y. Lin, and Y. Qing, "The clinical safety study of Mongolian medicine Garidi-5 pill containing Aconitum," *The Chinese Journal of Clinical Pharmacology*, vol. 28, no. 4, pp. 266–268, 2012.

[15] M. R. Zhi, S. Han, and K. Y. Liu, "Comparative study of cytotoxicity and anti-inflammatory effects between Raw Aconitium kusnezoffii and Aconitium kusnezoffii processed with Terminalia chebula," *China Pharmacy*, vol. 31, no. 22, pp. 2701–2705, 2020.

[16] S. Liu, X. Y. Liu, and Y. Li, "Experimental study on acute toxicity of the Aconiti kusnezoffii Radix and its processed products," *Chinese Journal of Pharmacovigilance*, vol. 12, no. 9, pp. 513–516+521, 2015.

[17] J.-H. Chen, C.-Y. Lee, B.-C. Liau, M.-R. Lee, T.-T. Jong, and S.-T. Chiang, "Determination of aconitine-type alkaloids as markers in fuzi (Aconitum carmichaeli) by LC/(+)ESI/MS3," *Journal of Pharmaceutical and Biomedical Analysis*, vol. 48, no. 4, pp. 1105–1111, 2008.

[18] J. Singhuber, M. Zhu, S. Prinz, and B. Kopp, "Aconitum in traditional Chinese medicine-A valuable drug or an unpredictable risk?" *Journal of Ethnopharmacology*, vol. 126, no. 1, pp. 18–30, 2009.

[19] T. Y. K. Chan, "Aconite poisoning," *Clinical Toxicology (Philadelphia, Pa.)*, vol. 47, no. 4, pp. 279–285, 2009.

[20] C.-C. Lin, T. Y. K. Chan, and J.-F. Deng, "Clinical features and management of herb-induced aconitine poisoning," *Annals of Emergency Medicine*, vol. 43, no. 5, pp. 574–579, 2004.

[21] L. Zhao, C. P. Liao, and X. J. Yang, "Research progress in Terminalia chebula and its predictive analysis on Q-marker," *Chinese Traditional and Herbal Drugs*, vol. 51, no. 10, pp. 2732–2744, 2020.

[22] X. H. Zheng, J. Yang, and Y. H. Yang, "Research progress on pharmacological effects of gallic acid," *Chinese Journal of Hospital Pharmacy*, vol. 37, no. 1, pp. 94–98+102, 2017.

[23] H. Y. Shi and Y. L. Chi, "Research progress in bioactivity of gallic acid," *Journal of Jilin Medical University*, vol. 41, no. 2, pp. 146–149, 2020.

[24] Y. y. Du, L. Zou, X. x. Wang, L. y. Dai, X. n. Ling, and Z. x. Xu, "Inhibitory effect of gallic acid on voltage-gated Na + channels in rat cardiomyocytes," *Clinical and Experimental Pharmacology and Physiology*, vol. 47, no. 5, pp. 771–779, 2020.

[25] R. Zhao and S. Y. Tsang, "Versatile roles of intracellularly located TRPV1 channel," *Journal of Cellular Physiology*, vol. 232, no. 8, pp. 1957–1965, 2017.

[26] R. Ramírez-Barrantes, C. Córdova, S. Gatica et al., "Transient receptor potential vanilloid 1 expression mediates capsaicin-induced cell death," *Frontiers in Physiology*, vol. 9, p. 682, 2018.

[27] B. F. Bessac and S. E. Jordt, "Breathtaking TRP channels: TRPA1 and TRPV1 in airway chemosensation and reflex control," *Physiology*, vol. 23, pp. 360–370, 2018.

[28] H. Shirakawa, T. Yamaoka, K. Sanpei, H. Sasaoka, T. Nakagawa, and S. Kaneko, "TRPV1 stimulation triggers apoptotic cell death of rat cortical neurons," *Biochemical and Biophysical Research Communications*, vol. 377, no. 4, pp. 1211–1215, 2008.

[29] J. Peng and Y. J. Li, "The vanilloid receptor TRPV1: role in cardiovascular and gastrointestinal protection," *European Journal of Pharmacology*, vol. 627, no. 1–3, pp. 1–7, 2010.

[30] M. J. Gunthorpe and A. Szallasi, "Peripheral TRPV1 receptors as targets for drug development: new molecules and mechanisms," *Current Pharmaceutical Design*, vol. 14, no. 1, pp. 32–41, 2008.

[31] Z. Sun, J. Han, W. Zhao et al., "TRPV1 activation exacerbates hypoxia/reoxygenation-induced apoptosis in H9C2 cells via calcium overload and mitochondrial dysfunction,"

International Journal of Molecular Sciences, vol. 15, no. 10, pp. 18362–18380, 2014.

[32] C. Wang, D. Sun, C. Liu et al., "Mother root of Aconitum carmichaelii Debeaux exerts antinociceptive effect in Complete Freund's Adjuvant-induced mice: roles of dynorphin/kappa-opioid system and transient receptor potential vanilloid type-1 ion channel," *Journal of Translational Medicine*, vol. 13, no. 1, p. 284, 2015.

[33] C. A. Yang, X. Y. Zeng, Z. F. Cheng, J. Zhu, and Y. Fu, "Aconitine induces TRPV2-mediated Ca^{2+} influx through the p38 MAPK signal and promotes cardiomyocyte apoptosis," *Evidence-based Complementary and Alternative Medicine*, vol. 2021, Article ID 9567056, 10 pages, 2021.

[34] Y. Li, J. Zeng, Y.-h. Tian et al., "Isolation, identification, and activity evaluation of diterpenoid alkaloids from Aconitum sinomontanum," *Phytochemistry*, vol. 190, Article ID 112880, 2021.

[35] S. Han, L. Y. Bao, and K. Y. Liu, "Mechanism of Aconiti Kusnezoffii Radix processed with Chebulae Fructus against h9c2 cardiomyocyte toxicity based on TRPV1 channel," *Chinese Journal of Experimental Traditional Medical Formulae*, vol. 28, no. 1, pp. 178–181, 2022.

[36] I. Zwolak, "Comparison of three different cell viability assays for evaluation of vanadyl sulphate cytotoxicity in a Chinese hamster ovary K1 cell line," *Toxicology and Industrial Health*, vol. 32, no. 6, pp. 1013–1025, 2016.

[37] H. Shan and N. Haridas, "Evaluation of clinical utility of serum enzymes and troponin-T in the early stages of acute myocardial infarction," *Indian Journal of Clinical Biochemistry*, vol. 18, no. 2, pp. 93–101, 2003.

[38] K. J. Valenzano, E. R. Grant, G. Wu et al., "N-(4-Tertiarybutylphenyl)-4-(3-chloropyridin-2-yl)tetrahydropyrazine -1(2H)-carbox-amide (BCTC), a novel, orally effective vanilloid receptor 1 antagonist with analgesic properties: I. In vitro characterization and pharmacokinetic properties," *Journal of Pharmacology and Experimental Therapeutics*, vol. 306, no. 1, pp. 377–386, 2003.

[39] C. M. Sag, A. C. Köhler, M. E. Anderson, J. Backs, and L. S. Maier, "CaMKII-dependent SR Ca leak contributes to doxorubicin-induced impaired Ca handling in isolated cardiac myocytes," *Journal of Molecular and Cellular Cardiology*, vol. 51, no. 5, pp. 749–759, 2011.

[40] S. Miyata, G. Takemura, K.-i. Kosai et al., "Anti-Fas gene therapy prevents doxorubicin-induced acute cardiotoxicity through mechanisms independent of apoptosis," *American Journal of Pathology*, vol. 176, no. 2, pp. 687–698, 2010.

[41] T. Kawada, T. Yamazaki, T. Akiyama, Y. Hayama, and M. Sugimachi, "Mild hypothermia is ineffective to protect against myocardial injury induced by chemical anoxia or forced calcium overload," *Journal of Cardiovascular Pharmacology*, vol. 73, no. 2, pp. 100–104, 2019.

[42] P. M. Sokolove and R. G. Shinaberry, "Na+-independent release of Ca^{2+} from rat heart mitochondria," *Biochemical Pharmacology*, vol. 37, no. 5, pp. 803–812, 1988.

[43] M. F. Chen, C. H. Ho, T. N. Tsai, P. S Chen, and S. J Chen, "Amiodarone for the successful management of Caowu poisoning-induced cardiac arrhythmia," *Acta Cardiologica Sinica*, vol. 34, no. 2, pp. 189–191, 2018.

[44] X.-c. Wang, Q.-z. Jia, Y.-l. Yu et al., "Inhibition of the INa/K and the activation of peak INa contribute to the arrhythmogenic effects of aconitine and mesaconitine in Guinea pigs," *Acta Pharmacologica Sinica*, vol. 42, no. 2, pp. 218–229, 2021.

[45] S. Liu, Y. Li, and W. F. Li, "Advances in studies on toxicity and modern toxicology of species in Aconitum L." *Chinese Traditional and Herbal Drugs*, vol. 47, no. 22, pp. 4095–4102, 2016.

[46] Q. Ye, H. Liu, C. Fang et al., "Cardiotoxicity evaluation and comparison of diterpene alkaloids on zebrafish," *Drug and Chemical Toxicology*, vol. 44, no. 3, pp. 294–301, 2021.

[47] L. Bartosova, F. Novak, M. Bebarova et al., "Antiarrhythmic effect of newly synthesized compound 44Bu on model of aconitine-induced arrhythmia—compared to lidocaine," *European Journal of Pharmacology*, vol. 575, no. 1–3, pp. 127–133, 2007.

[48] A. Ameri, "The effects of Aconitum alkaloids on the central nervous system," *Progress in Neurobiology*, vol. 56, no. 2, pp. 211–235, 1998.

[49] J. J. Wu, X. C. Wang, Y. Y. Chung et al., "L-type calcium channels inhibition contributes to the proarrhythmic effects of aconitine in human cardiomyocytes," *PLoS One*, vol. 12, no. 1, Article ID 168435, 2017.

[50] Y.-J. Wang, B.-S. Chen, M.-W. Lin et al., "Time-dependent block of ultrarapid-delayed rectifier K+ currents by aconitine, a potent cardiotoxin, in heart-derived H9c2 myoblasts and in neonatal rat ventricular myocytes," *Toxicological Sciences*, vol. 106, no. 2, pp. 454–463, 2008.

[51] T. Sawanobori, Y. Hirano, and M. Hiraoka, "Aconitine-induced delayed afterdepolarization in frog atrium and Guinea pig papillary muscles in the presence of low concentrations of Ca^{2+}," *The Japanese Journal of Physiology*, vol. 37, no. 1, pp. 59–79, 1987.

[52] Z. H. Liu, R. Guo, and W. Gao, "Effects of Wuzhuyu Decoction on visceral pain in mice through thermosensory channels TRPA1 and TRPV1," *China Journal of Traditional Chinese Medicine and Pharmacy*, vol. 35, no. 2, pp. 908–912, 2020.

[53] F. A. Fairin, A. E. Nugroho, and A. Nurrochmad, "Ginger extract and its compound, 6-shogaol, attenuates painful diabetic neuropathy in mice via reducing TRPV1 and NMDAR2B expressions in the spinal cord," *Journal of Ethnopharmacology*, vol. 249, Article ID 112396, 2020.

[54] Y. Yin, Y. Dong, S. Vu et al., "Structural mechanisms underlying activation of TRPV1 channels by pungent compounds in gingers," *British Journal of Pharmacology*, vol. 176, no. 17, pp. 3364–3377, 2019.

[55] H. Y. Zhou, L. Dai, and D. F. Wang, "Evaluation of regulational function of ingredients from hot herbs on TRPV1 channel based on 7900 PCR instrument," *Chinese Pharmacological Bulletin*, vol. 32, no. 10, pp. 1395–1398, 2016.

[56] S.-Q. Yu, S. Ma, and D. H. Wang, "TRPV1 activation prevents renal ischemia-reperfusion injury-induced increase in salt sensitivity by suppressing renal sympathetic nerve activity," *Current Hypertension Reviews*, vol. 16, no. 2, pp. 148–155, 2020.

[57] E. Iwaoka, S. Wang, N. Matsuyoshi et al., "Evodiamine suppresses capsaicin-induced thermal hyperalgesia through

activation and subsequent desensitization of the transient receptor potential V1 channels," *Journal of Natural Medicines*, vol. 70, no. 1, pp. 1–7, 2016.

[58] Z. Yang, *Study on the Influence of Lizhong Wan on the Thermal Channel TRPV1*, pp. 29–32, Heilongjiang University of Chinese Medicine, Heilongjiang, China, 2015.

[59] D. A. Simone, M. Nolano, T. Johnson, G. Wendelschafer-Crabb, and W. R. Kennedy, "Intradermal injection of capsaicin in humans produces degeneration and subsequent reinnervation of epidermal nerve fibers: correlation with sensory function," *Journal of Neuroscience*, vol. 18, no. 21, pp. 8947–8959, 1998.

[60] C. Tansen, L. M. N. Shimoda, and J. K. Kawakami, "Myrcene and terpene regulation of TRPV1," *Channels*, vol. 13, no. 1, pp. 344–366, 2019.

[61] X. Guo, M. L. Li, and X. L. Liu, "Effect of aconite containing serum on L-type calcium channel in rat ventricular myocytes," *Chinese Journal of Experimental Traditional Medical Formulae*, vol. 11, no. 21, pp. 111–115, 2015.